

Effect of electron-phonon interaction range on lattice polaron dynamics: a continuous-time quantum Monte Carlo study

P. E. Spencer,¹ J. H. Samson,¹ P. E. Komilovitch,^{2,y} and A. S. Alexandrov^{1,z}

¹Department of Physics, Loughborough University, Loughborough LE11 3TU, United Kingdom

²Hewlett-Packard Company, Mail Stop 321A, 1000 NE Circle Blvd, Corvallis, Oregon 97330, USA

(dated: May 23, 2019)

We present the numerically exact ground state energy, effective mass, and isotope exponents of a one-dimensional lattice polaron, valid for any range of electron-phonon interaction, applying a new continuous-time Quantum Monte Carlo (QMC) technique in a wide range of coupling strength and adiabatic ratio. The QMC method is free from any systematic finite-size and finite-time-step errors. We compare our numerically exact results with analytical weak-coupling theory and with the strong-coupling $1/\omega$ expansion. We show that the exact results agree well with the canonical Frohlich and Holstein-Lang-Firsov theories in the weak and strong coupling limits, respectively, for any range of interaction. We find a strong dependence of the polaron dynamics on the range of interaction. An increased range of interaction has a similar effect to an increased (less adiabatic) phonon frequency: specifically, a reduction in the effective mass.

I. INTRODUCTION

While qualitative features of polarons were well recognized a long time ago and have been described in several review papers and textbooks (see Ref. 1,2,3,4 for recent publications), there is renewed interest in quantitative studies owing to the overwhelming evidence for polaronic carriers in cuprates, fullerenes, and manganites (see, for example Ref. 3,4,5,6,7,8,9,10).

These "polaronic" conductors are quite different from ordinary metals. One can account for the electron-phonon (e-ph) interaction in simple metals by applying Migdal's theorem¹¹. The theorem shows that the contribution of diagrams with "crossing" phonon lines (so called "vertex" corrections) is small if the parameter $\lambda = E_F / \omega$ is small, where ω is the dimensionless (BCS) e-ph coupling constant, ω is the characteristic phonon frequency, and E_F the Fermi energy. Neglecting the vertex corrections Migdal calculated the renormalized electron mass as $m^* = m_0 (1 + \lambda)$ (near the Fermi level)¹¹, where m_0 is the band mass in the absence of the electron-phonon interaction, and Eliashberg¹² extended Migdal's theory to describe the BCS superconducting state at intermediate values of λ , $\lambda > 1$. Later on many authors applied the Migdal-Eliashberg theory with λ much larger than 1 (see, for example, Ref. 13).

On the other hand, starting from the infinite coupling limit, $\lambda = \infty$ and applying the inverse ($1/\omega$) expansion technique¹⁴ one can show^{15,16,17} that the many-electron system collapses into the small polaron regime at $\lambda \approx 1$ almost independently of the adiabatic ratio $\lambda = E_F / \omega$. This regime is beyond Migdal-Eliashberg theory. It cannot be reached by summation of the standard Feynman-Dyson perturbation diagrams even including all vertex corrections, because of the broken translational symmetry, as proposed by Landau¹⁸ for a single electron and by one of us¹⁵ for the many-electron system. A local translational-symmetry breaking drives the system into a new ground state at sufficiently large coupling, $\lambda > 1$. In this ground state the translational symmetry is restored but in a polaronic band rather than in the bare electron band. The non-adiabatic corrections (phonons) allow self-trapped polarons to propagate as Bloch waves in a new (narrow) band. In recent years many numerical and analytical studies have confirmed this conclusion (see Refs. 19,20,21,22,23,24,25,26,27,28,29,30,31,32,33,34 and references therein).

Hence, under certain conditions³⁴, the multipolaron system might be metallic but with polaronic (or bipolaronic) carriers rather than bare electrons. There is a qualitative difference between the ordinary metal and the polaronic one. In particular, the renormalized (effective) mass of electrons is independent of the ion mass M in ordinary metals (where the Migdal-adiabatic approximation is believed to be valid), because λ does not depend on the isotope mass. However, when the e-ph interaction is sufficiently strong, so that electrons form polarons dressed by lattice distortions, their effective mass m^* depends on M , $m^* = m_0 \exp(E_p / \omega)$, where E_p is the polaron level shift and is a numerical constant less than 1 (see below). Only the phonon frequency depends on the ion mass in m^* . Hence, there is a large isotope effect on the carrier mass in (bi)polaronic conductors, $m^* = (1/2) \ln(m^* / m)$, as predicted by one of us³⁵ in contrast to the zero isotope effect in ordinary metals. This effect has been found experimentally in cuprates¹⁰ and manganites³⁶. Recent high-resolution angle-resolved photoemission spectroscopy (ARPES)³⁷ provides further compelling evidence for a strong e-ph interaction in cuprates. It revealed the phonon structure in the electron self-energy of the underdoped $\text{La}_2 \times \text{Sr}_x \text{CuO}_4$ samples^{37,38}, and a complicated isotope effect depending on the electron energy and momentum in the electron spectral function of Bi2212³⁹. With increasing phonon frequency the range of validity of the $1/\omega$ polaron expansion extends to smaller values of λ ³⁴. As a result, the region of applicability of the Migdal-Eliashberg approach (even with vertex corrections) shrinks to smaller values of the coupling, $\lambda < 1$, with

increasing t . Strong correlations between carriers might reduce this region further²². Carriers in the fascinating novel materials are strongly coupled with high-frequency optical phonons, making polarons relevant for high-temperature superconductivity and colossal magnetoresistance phenomena.

Recent interest in polarons extends, of course, well beyond physical descriptions of materials. The field is a testing ground for analytical techniques, such as the $1/t$ diagrammatic expansion¹⁷, quantum-statistical mean-field models⁴⁰, different unitary transformations³⁰, dynamical mean-field theory²⁹, and numerical techniques, such as the numerical diagonalization of vibrating clusters^{20,22,23}, advanced variational methods^{4,27,28,31,32} and advanced quantum Monte Carlo (QMC) simulations^{41,42}.

In the framework of the single-polaron problem the most interesting (and difficult) question is the energy spectrum (effective mass) of the lattice polaron in the intermediate region of coupling and adiabatic ratio: $\beta \sim t^{-1}$ (where t is the hopping integral). To deal with this problem two of us (AK) proposed a one-dimensional model that can accommodate any range of e-ph interaction, suitable for exact QMC³³. The model was further studied by numerical cluster diagonalization⁴³ and $1/t$ expansion^{34,44}. The main conclusion was that the mass of the lattice polaron and the crossover from large to small polaron strongly depended on the range of the e-ph interaction. The small Frohlich polaron appeared to be lighter than the small Holstein polaron for the same binding energy by a few orders of magnitude with a gradual (rather than abrupt) self-trapping transition. Recently the AK model with two electrons has been studied variationally and by the $1/t$ expansion technique⁴⁵. Profound differences between the physical properties of bipolarons with Frohlich and Holstein interactions were found as well. In particular, the effective mass of the Frohlich bipolaron appeared to be much smaller than the Holstein (on-site) bipolaron mass. These and earlier studies (see, for example⁴⁶) of lattice polarons were mostly restricted to the Holstein⁴⁷ (zero range) and Frohlich⁴⁸ (infinite range) e-ph interactions.

In this paper we study the single polaron problem with the most physically realistic finite-range of interaction. We apply a new continuous-time QMC technique, developed by one of us⁴¹. This method is free from any systematic finite-size and finite-time-step errors and allows for (numerically) exact calculation of the ground-state energy and the effective mass of lattice polarons for any electron-phonon interaction. It does not involve Trotter slicing, providing an exact treatment of the kinetic energy. We introduce the electron-phonon Hamiltonian and AK model in section II. In section III we describe the continuous-time Monte Carlo scheme. In sections IV-VI we present the exact results for the energy, effective mass, number of dressing phonons, and isotope exponents of lattice polarons, compared with the canonical weak-coupling and strong-coupling analytical results for different interactions.

II. ELECTRON-PHONON MODEL

A. General model Hamiltonian

The electron-phonon model under investigation represents a single electron interacting with all the ions of an infinite hypercubic lattice, with one vibrational degree of freedom per unit cell. The generalized Hamiltonian reads^{33,41,47}

$$H = H_e + H_{ph} + H_{eph}; \quad (1)$$

where

$$H_e = \sum_{\langle nn^0 \rangle} t \sum_n c_n^\dagger c_{n^0}; \quad (2)$$

$$H_{ph} = \frac{1}{2M} \sum_m P_m^2 + \frac{M \omega_m^2}{2} \sum_m Q_m^2; \quad (3)$$

and

$$H_{eph} = \sum_{nm} f_m(n) c_n^\dagger c_{n-m}; \quad (4)$$

The free-electron term H_e describes the movement of a single electron through the lattice by the process of nearest-neighbor hopping. Here the operator c_n^\dagger creates an electron on site n , the operator c_{n^0} destroys an electron on site n^0 , and $\langle nn^0 \rangle$ denotes pairs of nearest-neighbor sites. In reciprocal space, this term is given by

$$H_e = \sum_k t_k c_k^\dagger c_k; \quad (5)$$

with free electron dispersion

$$\epsilon_k = \frac{\hbar^2 k^2}{2m} \quad (6)$$

Here a is the lattice constant, k is the wave vector of the electron, and d labels the component of the D dimensional hypercubic lattice.

The phonon term H_{ph} represents the vibrations of the lattice ions. Here the operator \hat{r}_m is the displacement of the m th ion from its equilibrium position, and $\hat{p}_m = i\hbar \nabla_m$ its momentum. It is assumed that the ions, each of ionic mass M , are non-interacting and so have the same characteristic (phonon) frequency ω . If \hat{c}_m^\dagger and \hat{c}_m are the creation and annihilation operators for a phonon of frequency ω on site m , then the phonon term is given by

$$H_{ph} = \sum_m \hbar \omega \left(\hat{c}_m^\dagger \hat{c}_m + \frac{1}{2} \right) \quad (7)$$

The final part of the Hamiltonian, the electron-phonon term H_{eph} , is of the "density-displacement" type, where the interaction energy between the electron and the m th ion is proportional to \hat{r}_m (the displacement of the m th ion from its equilibrium position). Here $\hat{c}_n^\dagger \hat{c}_n$ is the electron number operator, and $f_m(n)$ is interpreted as the interaction force between the electron on site n and the m th lattice ion. This interpretation can be understood from the following argument. Let U_{mn} be the work done in displacing the m th ion a small distance \hat{r}_m from its equilibrium position due to the presence of a carrier at site n . Then from first principles we may write $U_{mn} = f_m(n) \hat{r}_m$ where $f_m(n)$ is the internal "force" between the m th ion and the electron on site n . In second-quantized form this term is given by

$$H_{eph} = \sum_{nm} \frac{\hbar \omega}{2M \omega} f_m(n) \hat{c}_n^\dagger \hat{c}_n (\hat{c}_m^\dagger + \hat{c}_m) \quad (8)$$

The model is parameterized by two dimensionless quantities. The first is the dimensionless phonon frequency

$$\omega = \hbar \omega / zt \quad (9)$$

The second is related to the small-polaron binding energy E_p , derived in section (VI), which serves as a natural and convenient measure of the strength of the electron-phonon interaction. The dimensionless electron-phonon coupling constant is defined as

$$g = \frac{E_p}{zt} = \frac{1}{2M \omega zt} \sum_m f_m^2(0); \quad (10)$$

where zt is the bare-electron halfbandwidth, with z the lattice coordination number.

B. D discrete Frohlich model

Some time ago Alexandrov and Komilvitch proposed a long-range discrete Frohlich interaction³³ to describe the interaction between a hole and the apical oxygen ions in high- T_c superconducting materials. The model is depicted in FIG. 1 for the one-dimensional case. The mobile carrier (electron or hole) may hop from site to nearest-neighbor site along the lower chain. The chain consists of an infinite number of lattice sites with lattice constant a . The electron interacts with all the ions which reside at the lattice sites of a similar chain that is parallel to the first. The separation of the two chains is equal to the lattice constant a . We assume that the vibrations of the ions are polarized in a direction that is perpendicular to the chains, and that the ions do not interact with each other.

Let us find the appropriate form for the interaction force $f_m(n)$ between the mobile charge-carrier on the n th site (of the lower chain) and the m th ion (of the upper chain). Since both m and n are measured in units of a , we choose from this point on to take $a = 1$. The presence of the charge-carrier displaces the m th ion by a small distance \hat{r}_m in a direction perpendicular to the chain, as shown in FIG. 1. The distance between the charge-carrier and the displaced ion is

$$r_{mn}^0 = (m-n)^2 + (1-m)^2 = (m-n)^2 + 1 - 2m; \quad (11)$$

where only the first order terms in \hat{r}_m of the binomial expansion of $(1-m)^2$ have been retained. Using Coulomb's law, the difference in the mutual potential energy due to the change of radial distance r_{mn} to r_{mn}^0 is given by

$$U_{mn} = \frac{Q_m e}{4\pi\epsilon_0} \left(\frac{1}{r_{nm}^0} - \frac{1}{r_{nm}} \right); \quad (12)$$

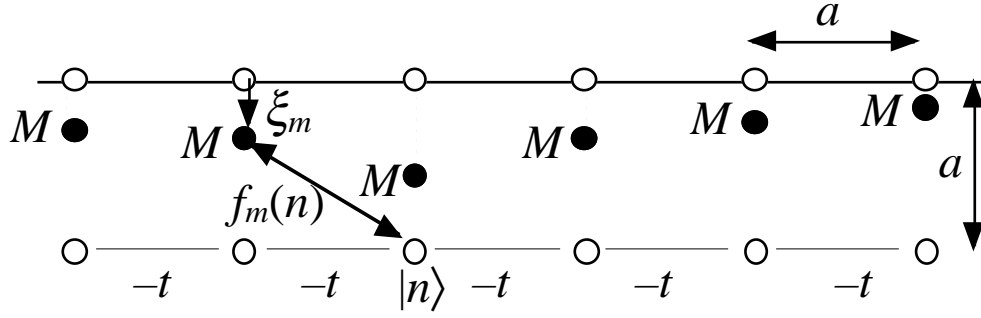


FIG. 1: Geometry of the Frohlich model (14) shown in one dimension. The mobile charge carrier m moves on the lower chain with nearest-neighbor hopping integral t and interacts with all the ions of the upper chain. The displacements ξ_m of the ions are polarized in a direction perpendicular to the chains.

where Q_m and e denote the charge of the ion and the charge-carrier respectively. We may use the binomial expansion again for the quantity $1/r_{nm}^0$, appearing in equation (12), to give

$$\frac{1}{r_{nm}^0} = \frac{1}{r_{nm}} \left[1 - \frac{2\xi_m}{r_{nm}} + \frac{3\xi_m^2}{r_{nm}^3} \right]; \quad (13)$$

where again we have kept only the first order terms in ξ_m . Thus, the difference in potential energy, which is due to the electron-phonon interaction only, can be written as

$$U_{mn} = \frac{Q_m e}{4\pi\epsilon_0} \frac{\xi_m}{[m - n]^2 + 1}^3; \quad (14)$$

This is the work done in taking the ion from its original position to its displaced position, and so $U_{mn} = f_m(n) \xi_m$, where $f_m(n)$ is the z -projection of the Coulomb force on the ion due to the presence of the carrier. Thus, we deduce that the Hamiltonian for the discrete Frohlich model is that of our generalized model Hamiltonian, Eq. 1, with the electron-phonon interaction force having the form

$$f_m(n) = \frac{Q_m e}{4\pi\epsilon_0} \frac{1}{[m - n]^2 + 1}^3; \quad (15)$$

with a constant ξ_m . Physically, this model was proposed in order to represent the interaction between a hole in the copper-oxygen layer (lower chain) and the apical oxygens in the ionic layer (upper chain) contained within the structure of certain doped high- T_c superconductors such as $YBa_2Cu_3O_{6+x}$ ³³. These materials are highly anisotropic due to the fact that the holes are sharply localized in the copper-oxygen layer, giving rise to poor conduction in the c -direction (normal to copper-oxygen layer). This leads to very poor screening of the electron-phonon interaction in the c -direction, and almost complete screening in the a - b plane. This justifies the restriction to phonon modes polarized in the c direction.

C. Screened Frohlich model

Our aim in this paper is to investigate the way in which the shape of the long-range electron-phonon interaction affects the properties of the polaron. It is therefore interesting to study the screened Frohlich model, in which the screening effect due to the presence of other electrons in the lattice is taken into account from within $f_m(n)$. Accordingly, let us define the interaction force for the screened Frohlich model as

$$f_m(n) = \frac{Q_m e}{4\pi\epsilon_0} \frac{1}{[m - n]^2 + 1}^3 \exp\left(-\frac{|m - n|}{R_{sc}}\right); \quad (16)$$

where R_{sc} is the screening length. That is, the screened force is the unscreened force multiplied by an exponential damping factor. Increasing the value of R_{sc} decreases the screening effect and thus increases the width of the interaction force.

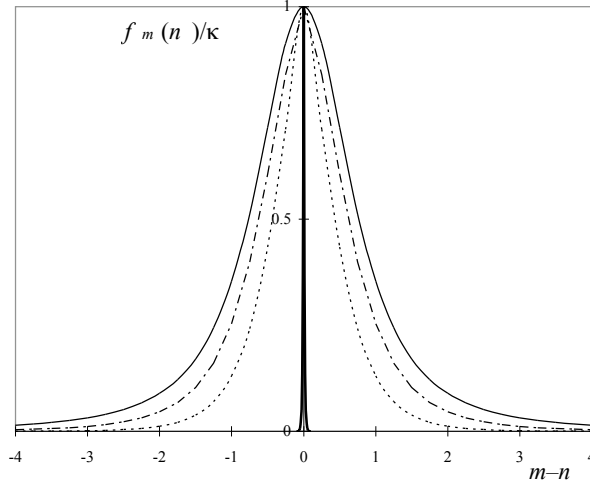


FIG. 2: The shape of the screened Frohlich interaction force, Eq. 16, at screening lengths of $R_{sc} \rightarrow 0$ (bold line, Holstein interaction), $R_{sc} = 1$ (dashed line), $R_{sc} = 3$ (dot-dashed line) and $R_{sc} \rightarrow \infty$ (thin line, non-screened Frohlich interaction).

The Holstein model describes an electron that interacts only with the oscillator it currently occupies ("short-range" interaction). This may be regarded as a special case of equation (16) with $R_{sc} \rightarrow 0$, so that $f_m(n) = \delta_{m-n}$.

Simply by altering the value of the parameter R_{sc} , we can easily transverse from the Holstein model, through the screened Frohlich model, to the non-screened Frohlich model, in a universal manner. In this paper we consider the following four cases in one dimension:

1. Holstein model with $R_{sc} \rightarrow 0$.
2. Screened Frohlich model, with $R_{sc} = 1$.
3. Screened Frohlich model, with $R_{sc} = 3$.
4. Non-screened Frohlich model with $R_{sc} \rightarrow \infty$.

The shapes of the electron-phonon interaction force $f_m(n)$ for each of the above screening lengths are shown in FIG. 2. Note that, based on calculations involving the dynamic properties of the polaron response³⁴, the amount of screening we impose here is greater than that expected in the high- T_c compounds.

III. PATH INTEGRAL APPROACH

A. Partition function

The partition function for our generalized model Hamiltonian is given by

$$Z = \int \prod_r d^N \mathbf{h} ; r j e^{-H_j ; r i} \quad (17)$$

where we have adopted the shorthand

$$Z = \int \prod_{m=1}^N d^N \mathbf{h}_m \quad (18)$$

Here we have summed over the discrete electron basis $|j_i\rangle$ and integrated over the continuous phonon basis $|j_i\rangle = |j_1; j_2; j_3; \dots; j_N\rangle$; In order to form the path integral of the partition function, the Boltzmann factor appearing in Eq. 17 is decomposed into L factors according to

$$e^{-H} = e^{-H_1} e^{-H_2} \dots e^{-H_L} \quad (19)$$

where we have defined

$$\Delta = \Delta L; \quad (20)$$

and then a complete set of states

$$\langle X | Z \rangle = \int_{r_1} d^N \langle j_{L+1}; r_{L+1} | \langle j_0; r_0 | \quad (21)$$

is inserted between each pair of factors (a total of $L - 1$ times). Thus the partition function in path integral representation is given by

$$Z = \int_{f_{r_1, g}} \langle X | Z \rangle = \int_{f_{r_1, g}} d^N \langle j_{L+1}; r_{L+1} | e^{-H} | j_0; r_0 \rangle; \quad (22)$$

where

$$\langle X | Z \rangle = \int_{f_{r_1, g}} d^N \langle j_{L+1}; r_{L+1} | Z | j_0; r_0 \rangle = \int_{f_{r_1, g}} \prod_{m=1}^L \prod_{l=0}^{L-1} d_{m, l}; \quad (23)$$

Note that the "end-states" in Eq. 22, namely $\langle j_{L+1}; r_{L+1} |$ and $| j_0; r_0 \rangle$, are identified with the states $\langle j; r |$ and $| j; r \rangle$ from Eq. 17.

The path integral has the following simple intuitive interpretation. One can think of the operator e^{-H} in Eq. 22 as an "imaginary time evolution operator" which propagates the system through an imaginary time interval of $\tau = \beta$. The formation of the path integral essentially introduces an imaginary time dimension $0 \leq l < L$, divided into L imaginary time slices, each of width $\Delta = \beta/L$ (labeled by index $0 \leq l < L$). Thus, r_l represents the position of the particle in the l 'th imaginary time slice, $d_{m, l}$ represents the displacement of the oscillator at site m in the l 'th time slice, and $f_{m, l}(r_l)$ is the force between the electron (at position r_l) and the m 'th ion in the l 'th imaginary time slice. Now, the set $f_{r_1, g}$ constitutes a single path or trajectory in imaginary time. The whole path integration is then just the sum over all the possible trajectories that takes the particle from the initial state $| j_0; r_0 \rangle$ (at imaginary time $\tau = 0$) to the final state $\langle j_L; r_L |$ (at imaginary time $\tau = \beta$). Each of the possible trajectories enters the path integration with a statistical weight given by

$$W = c_1 \langle j_{L+1}; r_{L+1} | e^{-H} | j_0; r_0 \rangle; \quad (24)$$

where c_1 is a constant (which is of little importance for our purposes as we will only require the ratio of weights).

The matrix elements appearing in Eq. 22 may be evaluated using the Trotter decomposition technique^{49,50}, which for our Hamiltonian produces

$$Z = \frac{M}{2^{\sim 2}} \int_{f_{r_1, g}} \prod_{l=0}^{L-1} \langle j_{L+1}; r_{L+1} | e^{-S} | j_0; r_0 \rangle; \quad (25)$$

Here the phonon action reads

$$S = \sum_{m=1}^N \sum_{l=0}^{L-1} \left[\frac{M}{2^{\sim 2}} (d_{m, l+1} - d_{m, l})^2 + \frac{M}{2} \sum_{m=1}^N d_{m, l}^2 + f_m(r_l) d_{m, l} \right]; \quad (26)$$

and the electronic contribution is represented by

$$I(r_{L+1}, r_0) = \frac{1}{N} \sum_k \cos[k \cdot (r_{L+1} - r_0)] \exp(-\epsilon_k); \quad (27)$$

where the free electron dispersion ϵ_k is defined in Eq. 6. This decomposition incurs a Trotter error (resulting from noncommutation of terms in the Hamiltonian), which vanishes in the limit $L \rightarrow \infty$.

B. Continuous imaginary time

QMC schemes have recently been developed that are implemented directly in continuous imaginary time for lattice models^{51,52,53}, eliminating the aforementioned Trotter finite-time-step error. In the limit of continuous imaginary time $L \rightarrow \infty$, our coordinates r_l and $r_{m,l}$ are replaced by the continuous functions of imaginary time $r(\tau)$ and $r_m(\tau)$ respectively. The path integration in Eq. 25 becomes

$$\lim_{L \rightarrow \infty} \int_{r_{1,0}}^{r_{1,L}} \int_{r_{2,0}}^{r_{2,L}} \dots \int_{r_{M,0}}^{r_{M,L}} d^N r = \int_{r(0)}^{r(L)} \int_{r_m(0)}^{r_m(L)} D r; \quad (28)$$

which represents integration over all possible trajectories that start with state $|j(0); r(0)\rangle$ and end with state $|j(L); r(L)\rangle$, and the phonon action is recast as

$$S = \sum_m S_m = \sum_m \int_0^L d\tau \left[\frac{M}{2\alpha^2} \dot{r}_m^2(\tau) + \frac{M}{2} \dot{r}_m^2(\tau) + f_m(r(\tau)) \right]; \quad (29)$$

where $\dot{r}_m(\tau) = \partial_\tau r_m(\tau) = \dot{r}_m$.

We wish to analytically integrate out the phonon degrees of freedom from the problem, that is, perform the phonon path integral

$$I = \int_{r(0)}^{r(L)} \int_{r_m(0)}^{r_m(L)} \exp(-S) D r; \quad (30)$$

As we shall see below, if the trajectory is measured from the classical (straight line) path, it turns out that the phonon coordinates enter the action only via the end-points of the trajectory, and the integration is easily performed in this Gaussian form.

The classical trajectory $r_m(\tau)$ may be determined by making use of the variational principle: of all of the possible trajectories $r_m(\tau)$, the classical path is that for which the action is an extremum⁵⁴. This path obeys the Euler-Lagrange equation

$$M \ddot{r}_m(\tau) + (\alpha^2)^{-1} r_m(\tau) = -\frac{\partial}{\partial r_m} f_m(r(\tau)); \quad (31)$$

This may be solved by using a Green's function to describe the particular non-homogeneous part of the solution⁵⁵ to give

$$r_m(\tau) = r_m(0) \frac{\sinh[\alpha(L-\tau)]}{\sinh(\alpha L)} + r_m(L) \frac{\sinh(\alpha \tau)}{\sinh(\alpha L)} + \frac{\alpha^{-2}}{M} \int_0^L d\tau' f_m(r(\tau')) G(\tau; \tau'); \quad (32)$$

where the Green's function reads

$$G(\tau; \tau') = \frac{1}{\alpha \sinh(\alpha L)} \begin{cases} \sinh(\alpha \tau) \sinh[\alpha(L-\tau')] & 0 < \tau < \tau' \\ \sinh[\alpha(L-\tau)] \sinh(\alpha \tau') & \tau' < \tau < L \end{cases}; \quad (33)$$

Here we have intentionally not imposed any boundary conditions on the start, $r_m(0) = r_m(0)$, and end, $r_m(L) = r_m(L)$, of the trajectory at this stage.

Let us decompose the trajectory $r_m(\tau)$ according to

$$r_m(\tau) = r_m^{\text{cl}}(\tau) + \delta r_m(\tau); \quad (34)$$

where the classical path $r_m^{\text{cl}}(\tau)$ is given by Eq. 32, and $\delta r_m(\tau)$ is the deviation from $r_m^{\text{cl}}(\tau)$ (quantum fluctuation). This is reasonable because the probability amplitude for the trajectories to be "close" to the classical path is large, and becomes smaller as the difference between the two increases. Using this decomposition, the classical part of the action in Eq. 29 is expressed in terms of the phonon coordinates of the end-points only as

$$S_m^{\text{cl}} = \frac{M}{2\alpha \sinh(\alpha L)} \left[\dot{r}_m^2(0) + \dot{r}_m^2(L) \right] \cosh(\alpha L) + 2 r_m(0) \dot{r}_m(L) + r_m(0) B_m(L) + r_m(L) C_m(L) + \frac{\alpha^{-2}}{2M} \int_0^L \int_0^L d\tau d\tau' f_m(r(\tau)) G(\tau; \tau') f_m(r(\tau')); \quad (35)$$

where

$$B_m(\mathbf{r}) = \int_0^Z d\tilde{r} \frac{\sinh(\tilde{r} \cdot \mathbf{r})}{\sinh(\tilde{r})} f_m(\mathbf{r}(\tilde{r})); \quad (36)$$

and

$$C_m(\mathbf{r}) = \int_0^Z d\tilde{r} \frac{\sinh(\tilde{r} \cdot \mathbf{r})}{\sinh(\tilde{r})} f_m(\mathbf{r}(\tilde{r})); \quad (37)$$

The fluctuation part is quadratic in $m(\mathbf{r})$ and decouples from the classical path, giving only a constant normalization factor to the path integral.

According to Eq. 22, we require the phonon path integral, Eq. 30, to be performed using periodic boundary conditions in imaginary time, that is

$$m(0) = m(\beta) = m; \quad (38)$$

Under this condition one can see that S_m , equation (35), depends on a single phonon coordinate m only. Thus the "phonon path integral for periodic boundary conditions" I_{per} decomposes into the product of one-variable Gaussian integrals

$$I_{\text{per}} = \prod_m \int_{-\infty}^{\infty} d m \exp(S_m); \quad (39)$$

which can easily be performed to give

$$I_{\text{per}} = \frac{\int_{-\infty}^{\infty} d m \exp(S_m)}{M! [\cosh(\tilde{r}) - 1]^{N=2}} \exp(A_{\text{per}}); \quad (40)$$

where

$$A_{\text{per}} = \frac{\int_0^Z \int_0^Z d\tilde{r} d\tilde{r}' \frac{\cosh[\tilde{r} \cdot (\mathbf{r} - \mathbf{r}')]}{\sinh(\tilde{r} - \tilde{r}')}}{4M!} f_m(\mathbf{r}(\tilde{r})) f_m(\mathbf{r}(\tilde{r}')); \quad (41)$$

which does not contain any phonon degrees of freedom. We have thus transformed the problem from that of an electron interacting with M many phonons to that of an electron with retarded self-interaction, which allows the QMC method to be applied effectively.

C. Effective mass using twisted boundary conditions

Let us define the polaron dispersion $E_0(\mathbf{P})$ to be the lowest energy state of the system of total electron-phonon momentum \mathbf{P} . This is well defined where the force $f_m(\mathbf{r})$ is a function of m only, as the Hamiltonian \mathcal{H} then commutes with \mathbf{P} . If the ground state has zero momentum, the expansion

$$E_0(\mathbf{P}) = E_0(0) + \frac{1}{2} (m^{-1})_{ij}^1 P_i P_j + \dots; \quad (42)$$

defines the effective mass tensor m^{-1} . In the isotropic (or one-dimensional) case this is

$$E_0(\mathbf{P}) = E_0(0) + \frac{P^2}{2m} + \dots; \quad (43)$$

Given a Monte Carlo evaluation of the energy $E(\mathbf{P})$ at finite inverse temperature we have

$$(m^{-1})_{ij}^1 = \lim_{\beta \rightarrow \infty} \frac{\partial^2 E(\mathbf{P})}{\partial P_i \partial P_j}; \quad (44)$$

or

$$(m^{-1})^1 = \lim_{\beta \rightarrow \infty} \frac{\partial^2 E(\mathbf{P})}{\partial P^2}; \quad (45)$$

The above definitions do not provide a practical means of evaluating the effective mass, since a minus-sign problem arises for finite momentum, exacerbating the errors inherent in differentiating QMC energies. Obtaining dynamical properties such as the effective mass from QMC usually involves some kind of analytical continuation from imaginary to real time. The effective mass may however be inferred directly from QMC simulation by considering electron trajectories with twisted (rather than periodic) boundary conditions in imaginary time. To demonstrate this we decompose the partition function according to

$$Z = \sum_P Z_P; \quad (46)$$

where the partial partition function

$$Z_P = \sum_i \langle i | e^{-\beta H} | j \rangle_{P, P_i} \quad (47)$$

involves only those states with a fixed total momentum P . Here i numbers states of a complete basis (of momentum eigenstates), and P_i is the total momentum of state j . This decomposition is possible because, as in any translationally invariant system, the total momentum is conserved (within the first Brillouin zone), and so trajectories that have an initial total momentum P_i will evolve and end with the same P_i . Komilovitch⁴¹ showed that

$$Z_P = \sum_r e^{iP \cdot r} Z_r; \quad (48)$$

with

$$Z_r = \sum_{\{r\}} \langle f_{m+r} | e^{-\beta H} | f_m \rangle_{r; r_i} \quad (49)$$

where the summation includes all possible values of $r = r^0 + r$. Now, a comparison of Eqs. 17 and 48 shows that the above derivation of S_m as in Eq. 35 for Z is also appropriate for Z_P , up to the weight factor $e^{iP \cdot r}$, by imposing twisted boundary conditions in imaginary time

$$\begin{aligned} \langle f_m(0) | g; r(0) \rangle &= \langle f_m | g; r_i \rangle \\ \langle f_m(\beta) | g; r(\beta) \rangle &= \langle f_{m+r} | g; r + r_i \rangle \end{aligned} \quad (50)$$

That is, the final state ($= \beta$) is the initial state ($= 0$) with all the coordinates (electron and all phonons) shifted by r .

In this paper we will consider the case of $P = 0$, for which the factor $e^{iP \cdot r}$ is always unity, and so

$$Z_{P=0} = \sum_r Z_r; \quad (51)$$

The QMC weight is always positive-definite for $P = 0$, and so the troublesome sign problem is avoided (the case for non-zero P was considered by Komilovitch⁵⁶ in order to determine the whole polaron spectrum $E_0(P) - E_0(0)$). The effective mass is defined in the limit $\beta \rightarrow \infty$, in which limit the partition function is dominated by the lowest eigenstate:

$$Z_P \sim e^{-\beta E_0(P)} \text{ as } \beta \rightarrow \infty; \quad (52)$$

Expanding Eqs. 52 and 48 to second order in P yields

$$m_0^{-1}(\mathbf{m})_{ij}^{-1} = \frac{1}{2\tau a^2} \frac{\sum_r r_i r_j Z_r}{\sum_r Z_r}; \quad (53)$$

or

$$\frac{m_0}{m} = \frac{1}{2\tau a^2} \frac{\sum_r \langle r \rangle^2 Z_r}{\sum_r Z_r} \quad (54)$$

in the isotropic or one-dimensional case, where the bare electron mass is

$$m_0 = \frac{\hbar^2}{2\tau a^2}; \quad (55)$$

The statistical average of $(r)^2$ over trajectories at $P = 0$ is easily obtainable from QMC simulation.

Let us now integrate out the phonon degrees of freedom from the system using twisted boundary conditions in imaginary time, that is, perform the phonon path integral, Eq. 30, over all trajectories subject to the constraint

$$m(0) = m; \quad m(\tau) = m + r : \quad (56)$$

On imposition of these boundary conditions, the action S_q includes a mixed variable term involving m and $m + r$, and so Gaussian integration can not be applied directly (as was the case for periodic boundary conditions). However, we may proceed by transforming m and $m + r$ into real Fourier components a_q and b_q using a transformation of the form

$$m = \frac{1}{\sqrt{DN}} \sum_q (a_q + ib_q) e^{iqm} ; \quad (57)$$

and so

$$m + r = \frac{1}{\sqrt{DN}} \sum_q (a_q + ib_q) e^{iq(m+r)} ; \quad (58)$$

where D is the dimensionality of the lattice and DN is the total number of phonon degrees of freedom. In this representation, the action is diagonal (involves no mixed terms) and thus the "phonon path integral for twisted boundary conditions" I_{tw} decomposes according to

$$\begin{aligned} I_{tw} &= \int \prod_q da_q db_q \exp \left(\sum_q S_q \right) \\ &= \int \prod_q da_q db_q \exp (S_q) : \end{aligned} \quad (59)$$

After performing the Gaussian integral the result is

$$I_{tw} = \frac{\sim \sinh(\tau)}{M! [\cosh(\tau) \cos(qr)]^{DN/2}} \exp A_{tw} ; \quad (60)$$

where

$$\begin{aligned} A_{tw} &= \frac{\sim \sinh(\tau)}{2M! [\cosh(\tau) \cos(qr)]^P} \sum_m B_m (C_{m+r} - C_m) + \frac{\sim \sinh(\tau)}{4M! [\cosh(\tau) \cos(qr)]^P} \sum_m (B_m + C_m)^2 \\ &\quad + \sum_m \frac{\tau^2}{2M} \int_0^{\tau} \int_0^{\tau} d\tau' d\tau'' f_m(r(\tau')) G(\tau'; \tau'') f(r(\tau'')) ; \end{aligned} \quad (61)$$

which contains no phonon degrees of freedom, and correctly reduces to Eq. 41 for $r = 0$.

Finally, the result above may be conveniently rendered into the required low temperature limit using

$$\cosh \tau \sim \sinh \tau \sim \frac{1}{2} e^{\tau} \quad ; \quad (62)$$

which gives

$$I_{tw} / \exp A_{tw} = \exp (A_{per} + A) ; \quad (63)$$

where

$$A_{per} = \frac{\tau!}{2 \int_0^{\tau} \int_0^{\tau} d\tau' d\tau'' e^{-(\tau-j\tau')} + e^{-(\tau-j\tau'')} \int_0^{\tau} \int_0^{\tau} f(r(\tau)); r(\tau'')) \quad (64)$$

is the low temperature action for periodic boundary conditions, and

$$A = \frac{\tau!}{\int_0^{\tau} \int_0^{\tau} d\tau' d\tau'' e^{-(\tau-j\tau')} [\int_0^{\tau} f(r(\tau)); r(\tau'')) \int_0^{\tau} f(r(\tau)); r(\tau'')) \quad (65)$$

is the correction for twisted boundary conditions, in dimensionless form. Here $\tau = t$ and $\tau_0 = t_0$ are dimensionless imaginary time; the parameters τ and τ_0 are defined in Eqs. 9 and 10 respectively; and the lattice summation is defined as

$$\sum_r (r(\tau); r(\tau_0)) = \sum_m f_m(r(\tau)) f_{m+r}(r(\tau_0)); \quad (66)$$

Note that the dimensionless quantity $f_m(n)$ represents the shape or form of the electron-phonon interaction force, defined via the decomposition

$$f_m(n) = f_m(n); \quad (67)$$

where $\tau = 2z M t^3 \tau_0^2 = \tau_0^2 \sum_m f_m^2(0) \tau_0^{-1}$ takes the dimensions of force.

IV. CONTINUOUS-TIME MONTE CARLO

A. Algorithm

Traditionally, path-integral QMC simulation is implemented in discrete imaginary-time, where the trajectory is represented by the position of the electron in each of a large number of imaginary-time slices. The use of discrete time introduces the problematic finite-time-step systematic error, which scales with the square of the time-slice-width.

Recently a path-integral QMC scheme that is implemented directly in continuous imaginary-time has been developed for systems with a discrete basis^{52,53}. Here, the electron trajectory is represented as finite intervals of imaginary time in which the system remains in a particular state, separated by sporadic transitions from one state to another (an electron hop). The points in imaginary time at which the state of the system changes are called "kinks", as shown in FIG. 3. It is necessary to consider the statistics governing different directions of kink independently of one another. For our one-dimensional case with nearest-neighbor-hopping, we need only consider single left and right kinks. The use of continuous time completely eliminates the finite-time-step error, rendering the scheme "numerically exact".

If N_s is the number of kinks of direction s , we wish to generate random states according to the Monte Carlo weight

$$w(N_s) = w_{el}(N_s) w_{ph}(N_s); \quad (68)$$

where the weight from the electron subsystem

$$w_{el}(N_s) = \sum_s \frac{(t)^{N_s} e^{-t}}{N_s!} \quad (69)$$

is given by the Poisson distribution, and the phonon-induced weight

$$w_{ph}(N_s) = \exp[-A_{tw}(N_s)] \quad (70)$$

is given by Eq. 63.

Proposed changes to the shape of the trajectory are generated by the addition or deletion of single kinks. This is sufficient in practice. In order to increase efficiency one might also consider: changing a kink-direction, repositioning a kink in imaginary-time, or altering the temporal ordering of the kinks. The Metropolis method^{57,58} accepts or rejects the trial change from state N_s to state $N_s \pm 1$ with a transition probability $P(N_s \pm 1) = g(N_s \pm 1) a(N_s \pm 1)$, where $g(N_s \pm 1)$ is the sampling distribution and $a(N_s \pm 1)$ as the acceptance probability. For the case of $N_s \pm 1$ (one or more kinks exist), we choose $g(N_s + 1) = g(N_s) = 1/2$, and so the acceptance probability is given by

$$a_{add}(N_s \rightarrow N_s + 1) = \min \left[1, \frac{g(N_s + 1) W(N_s + 1)}{g(N_s) W(N_s)} \right] \quad (71)$$

$$= \min \left[1, \frac{t}{N_s + 1} \exp[A_{tw}(N_s + 1) - A_{tw}(N_s)] \right] \quad (72)$$

to add a kink, and similarly

$$a_{rem}(N_s + 1 \rightarrow N_s) = \min \left[1, \frac{N_s + 1}{t} \exp[A_{tw}(N_s) - A_{tw}(N_s + 1)] \right] \quad (73)$$

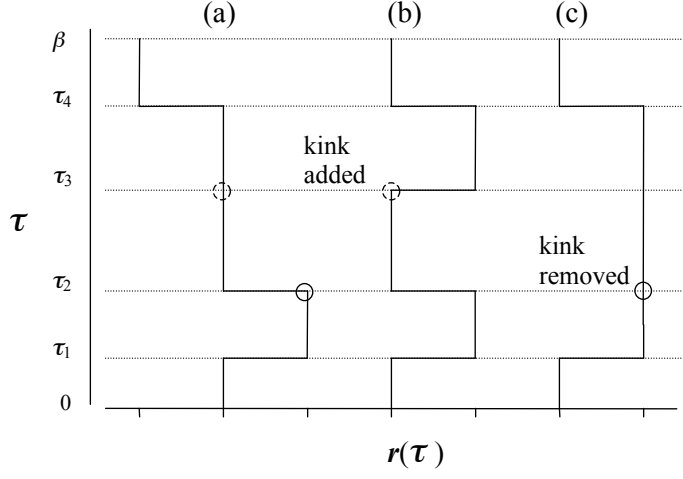


FIG. 3: Illustration of a one-dimensional electron trajectory in imaginary time. The point in imaginary time at which the electron hops to a neighboring site is known as a kink. (a) Shows a trajectory with three kinks: occurring at τ_1 , τ_2 , and τ_3 . (b) The same trajectory, but with a kink added at time τ_3 . The entire trajectory above τ_3 is shifted by one lattice parameter. (c) The same trajectory as in (a) but with the kink at τ_2 removed. A gain, the entire trajectory above τ_2 is shifted accordingly.

to remove a kink of direction s . For the case of $N_s = 0$, we can only add a kink, and so $g(0 \rightarrow 1) = 1$, which gives

$$a_{\text{add}}(0 \rightarrow 1) = \min \left[1; \frac{t}{2} \exp [A_{\text{tw}}(1) - A_{\text{tw}}(0)] \right] \quad (74)$$

and

$$a_{\text{rem}}(1 \rightarrow 0) = \min \left[1; \frac{2}{t} \exp [A_{\text{tw}}(0) - A_{\text{tw}}(1)] \right] : \quad (75)$$

The continuous-imaginary-time QMC step used in this work has the following structure:

1. Randomly select a kink direction s for the trial change. In the case of a one-dimensional system, this is left or right.
2. Propose a change to the trajectory by randomly selecting whether to add a new kink (at a random imaginary time) or to remove an existing kink (selected in a random fashion). This is done according to the selection probabilities $g(N_s + 1 \rightarrow N_s)$ and $g(N_s \rightarrow N_s + 1)$.
3. Accept or reject the proposed change with probability $a_{\text{add}}(N_s \rightarrow N_s + 1)$ if adding, or $a_{\text{rem}}(N_s + 1 \rightarrow N_s)$ if removing a kink.
4. If the change has been accepted, then the entire trajectory that lies "above" the kink (i.e. from the imaginary time of the kink to β) is shifted across accordingly. If the proposed change has been rejected, then the trajectory is left untouched.

B. Analytical integration over kinks

The Metropolis algorithm requires the action, which involves a double integration in imaginary time, to be computed on each Monte Carlo step. The fact that the trajectory consists of a series of single kinks, between which the trajectory

is a straight line, allow us to "break up" the area of integration into segments, such that the integration can be treated analytically within each segment. The action can thus be computed efficiently using a double summation over kinks.

The integration appearing in Eqs. 64 and 65 can be broken up using

$$\int_0^Z \int_0^Z d\mathbf{d}^0 = \sum_{j=1}^{N_x+1} \sum_{k=1}^{N_x+1} \int_{j_1}^{j_2} \int_{k_1}^{k_2} d\mathbf{d}^0; \quad (76)$$

The diagonal and off-diagonal segments can be treated separately in order to reduce computation. Each rectangular segment is specified by four times, $[j_1; j_2; k_1; k_2]$, each of which correspond to the position of a kink in imaginary-time. In the range $[j_1; j_2]$, the position of the electron is fixed at $r(\cdot) = r(j_1)$, and similarly in the range $[k_1; k_2]$, the position $r(\cdot) = r(k_1)$ is fixed. Thus, within each segment the lattice summation

$$r(r(j_1); r(k_1)) = \sum_m f_m(r(j_1)) f_{m+r}(r(k_1)); \quad (77)$$

has a constant value. Thus, the double integral in the action can be treated analytically within each segment to give

$$A_{tw} = \sum_{j=1}^{N_x+1} \sum_{k=1}^{N_x+1} A_{jk}; \quad (78)$$

where

$$A_{jk} = \frac{Z}{2!} \frac{h}{(0;0)} K(j; j_1) K(k; k_1) e^{-(k_1 - j_1) \phi(r(j_1); r(k_1))} + e^{-(k_1 + j_1) \phi(r(j_1); r(k_1))}; \quad (79)$$

with

$$K(j; j_1) = 1 - e^{-(j - j_1) \phi}; \quad (80)$$

For the models studied in this paper, $f_m(n)$ depends only on the relative lattice distance $j_n - n_j$ and tends to zero (or is zero) at large distance. Consequently, the lattice summation is a function of the single variable $r^0 = r_2 - r_1 - r$ only, namely

$$r(r^0) = \sum_{m^0} f(m^0) f(m^0 - r^0); \quad (81)$$

which can be evaluated for all possible values of r^0 in advance of the simulation proper.

C. Physical Observables

We consider four physical observables: the ground state energy, the number of phonons in the polaron cloud, the effective mass, and the isotope exponent on the effective mass. For a given observable Q , the expectation value is the statistical average over trajectories at $P = 0$ (ground state), which can be written in the form

$$\langle Q \rangle_{i_0} = \frac{\int_{tw} D\mathbf{r} Q w(N_s)}{\int_{tw} D\mathbf{r} w(N_s)}; \quad (82)$$

where the phonon degrees of freedom have been integrated out, and $w(N_s)$ is given by Eq. 68. This corresponds to a simple arithmetic average within the QMC simulation.

The ground state ($P = 0$) energy estimator is given by⁴¹

$$E_0(0) = \frac{1}{w} \frac{\partial w}{\partial \beta_0} = \frac{\partial A}{\partial \beta_0} = \frac{1}{s} \sum_s^* N_s; \quad (83)$$

which follows the corresponding finite-imaginary-time energy estimator⁴⁹ in the continuum limit.

The number of phonons in the polaron cloud N_{ph} quantifies the amount of lattice deformation associated with the polaron. The value of N_{ph} is given by the expectation value of the phonon number operator, which can be isolated from the model Hamiltonian by taking its partial derivative with respect to ω_m (holding ω_m constant), that is

$$\frac{\partial H}{\partial \omega_m} = \sum_m \alpha_m^y d_m : \quad (84)$$

This can be related to the action via the free energy $F_0 = -k_B T \ln Z_0$ to give

$$N_{ph} = \sum_m \alpha_m^y d_m = \frac{\partial F_0}{\partial \omega_m} = \frac{1}{k_B T} \frac{\partial A}{\partial \omega_m} : \quad (85)$$

We showed in the previous section that, by imposing twisted (rather than periodic) boundary conditions in imaginary time, the effective mass (second-order quantity in P) can be inferred directly from QMC simulation. The inverse effective mass of the polaron, Eq. 53, may be written as

$$\frac{m_{0;d}}{m_d} = \frac{1}{2} \frac{D}{(r_d)^2} \frac{E}{\omega_m} ; \quad (86)$$

where the difference in position of the endpoints of the trajectory $r_d = r_d(\tau) - r_d(0)$ is measured in units of the lattice constant a , m_d is the effective mass, and $m_{0;d}$ the bare electron mass, where d labels the dimension of the D -dimensional system.

The isotope effect is most often observed via its influence on the superconducting transition temperature T_c . The dependence of T_c on the mass of the lattice ions M has been found empirically to be T_c / M^{α} ,^{59,60} where α is known as the isotope exponent on T_c . In a similar way, let us define the isotope exponent on the effective mass m as

$$\alpha_m^{(d)} = \frac{M}{m_d} \frac{dm_d}{dM} = M \frac{m_d}{m_{0;d}} \frac{\partial}{\partial M} \frac{m_{0;d}}{m_d} : \quad (87)$$

On substitution of the derivative of $m_{0;d} = m_d$, as in Eq. 86, with respect to M , we get

$$\alpha_m^{(d)} = \frac{1}{2} \frac{D}{(r_d)^2} \frac{E}{\omega_m} \frac{\partial \omega_m}{\partial M} = \frac{1}{2} \frac{D}{(r_d)^2} \frac{E}{\omega_m} \frac{\partial \omega_m}{\partial M} ; \quad (88)$$

where the ionic mass enters our formalism via the phonon frequency $\omega_m = (k/M)^{1/2}$, where k is some "spring constant".

The expectation values, then, depend on the difference in position of the endpoints r_d , and partial derivatives of the action in Eq. 63 with respect to either ω_m or ω_m (holding the other model parameters constant). After performing the differentiation analytically, the resulting expressions are easily incorporated into the QMC scheme.

For each model, simulations were conducted for various different values of the dimensionless parameters ω_m and ω_m . A typical QMC simulation consisted of a series of between 10^6 and 6×10^6 measurements, taken every 10 to 50 Monte Carlo steps (to reduce statistical correlation). For each set of model parameters ($\epsilon_m(n)$, ω_m and ω_m), between 3 and 6 statistically independent simulations were performed, each using a different value of the inverse temperature β . Values of β in the range 15 to 25 were found to be sufficient to enforce the low-temperature limit $\exp(\beta \epsilon_m) \gg 1$. Averages included only those measurements taken after the system was judged to have reached equilibrium. In most cases, the Monte Carlo averages were determined to a statistical error of less than one percent.

V. LIMITING CASES

A. Strong Coupling (Small Polaron) Regime

When the electron-phonon coupling is strong, the electron becomes "trapped" in a potential well created by the induced lattice distortion. In this case the "size" of the polaron state can become comparable with the lattice constant, and the term "small polaron" is used. The condition for small polaron formation is $\epsilon_p = E_p = zt \gg 1$, which is referred to as the strong-coupling regime⁶¹. The small polaron can move from site to site (at zero temperature) through the action of zero-point motion.

An analytical method to determine the effective mass and energy dispersion in the strong-coupling regime, for a lattice polaron with a general electron-phonon interaction force $f_m(n)^{33}$, is based on the Lang-Firsov canonical transformation¹⁴ (which renders the transformed Hamiltonian diagonal for $\beta \rightarrow 1$), followed by a second-order perturbation technique that uses β as a small parameter⁶¹. For nearest-neighbor hopping only, and forms of $f_m(n)$ that depend on the relative lattice distance $j_n - n_j$, the result for the lowest energy levels reads³³

$$E(k) = E_p + \epsilon_p(k) \sum_{k^0; n_q} \frac{\sum_{j; n_n^0} t_{jn^0} \exp \sum_{m,q} \frac{(f_m(n) - f_m(n^0)) (e^{iq \cdot m} d_q^y - e^{-iq \cdot m} d_q)}{2NM \sim! q^3} c_{n^0}^y c_{n_q}^y}{\sim! q n_q}; \quad (89)$$

where the summation is over intermediate states with one or more phonons, $\sum_{q n_q}^P q n_q > 0$, the polaronic energy-level shift

$$E_p = \frac{1}{2M \sim!^2} \sum_m f_m^2(0) \quad (90)$$

(used to define ϵ_p) corresponds with the solution for $\beta \rightarrow 1$, and the small-polaron dispersion

$$\epsilon_p(k) = t \sum_{n \in 0} e^{g^2(1)} e^{ik \cdot n}; \quad (91)$$

where g^2 is known as the (zero temperature) mass renormalisation exponent, given by

$$g^2(1) = \frac{1}{2M \sim!^3} \sum_m f_m^2(0) f_m(0) f_m(1); \quad (92)$$

The final term of Eq. 89 is quadratic with respect to the bare hopping amplitude t_{jn^0} , and produces a negative correction to the energy. (Here, n_q is the number of phonons with wave vector q , and $j k^0; n_q i$ is an excited state that consists of a single electron with wave vector k^0 and one or more phonons.) It is of order of β^{-2} and is almost independent of k ³³.

In the ground state of the system ($k = 0$), the value of $\epsilon_p(k)$ is real and small compared with E_p , and so Eq. 89 is dominated by E_p . Thus, the (dimensionless) strong-coupling result for the ground state energy is

$$\frac{E_0}{t} = z; \quad (93)$$

and since $E_p = N_{ph} \sim!$, it follows that the number of phonons in the polaron cloud at $k = 0$ is given by

$$N_{ph} = \frac{z}{!}; \quad (94)$$

Assuming that the third term in Eq. 89 is completely independent of k , then the inverse effective mass, for the isotropic or one-dimensional case, is given by

$$\frac{m_0}{m} = m_0 \frac{\partial^2 E_k}{\partial k^2} \Big|_{k=0} = e^{g^2(1)}; \quad (95)$$

This can be conveniently expressed in dimensionless form as

$$\frac{m_0}{m} = \exp \frac{2}{!}; \quad (96)$$

where we have defined the constant

$$1 = \frac{P}{m_0} \frac{f_m(0) f_m(1)}{f_m^2(0)}; \quad (97)$$

which depends only on the shape of the electron-phonon interaction force. The isotope exponent on the effective mass m , defined in Eq. 87, can be written in terms of $! / M^{1=2}$ as

$$m = \frac{m_0}{2} \frac{\partial}{\partial !} \frac{m_0}{m}; \quad (98)$$

for the isotropic (or one-dimensional) case. Thus, the (dimensionless) strong-coupling isotope exponent is given by³⁵

$$m = \frac{!}{!}; \quad (99)$$

The value of the dimensionless constant $0 < 1$ must in general be determined numerically: the value calculated for each of the one-dimensional interaction models studied in this work is presented in TABLE I.

Interaction Model	
Holstein	1.000
Screened Frohlich ($R_{sc} = 1$)	0.745
Screened Frohlich ($R_{sc} = 3$)	0.531
Non-screened Frohlich	0.387

TABLE I: Values of the dimensionless parameter $\gamma = \frac{1}{m} \sum_m f_m(0) f_m(1) = \frac{1}{m_0} \sum_m f_m^2(0)$ for the one-dimensional models studied in this work, where γ depends only on the shape of the interaction force.

B. Weak Coupling (Large Polaron) Regime

In 1950 Frohlich et al.⁶² considered the ground state of a polaron in the weak-coupling limit $\gamma \ll 1$, using second-order perturbation theory, under the condition that there is never more than one phonon virtually excited, and the discreteness of the lattice is unimportant (because the band-electron-like "large polaron" state⁶³ is much larger than the lattice constant). Thus we write

$$H = H_0 + H_{eph}; \quad (100)$$

where H_{eph} is a small perturbation on

$$H_0 = \frac{\hbar^2 k^2}{2m_0} + \sum_q \tilde{c}_q^\dagger c_q; \quad (101)$$

Assuming that $f_m(n)$ depends only on the relative lattice distance $|m-n|$, equation (100) may be written in momentum representation as

$$H_{eph} = \sum_{q;k} \tilde{c}_q^\dagger \tilde{c}_k c_k c_q^\dagger + \text{h.c.}; \quad (102)$$

where we have defined $\tilde{c}_q = \sum_r c_{r-m} e^{iq \cdot r}$ and

$$\tilde{c}_q = \sum_r f_r(0) e^{iq \cdot r}; \quad (103)$$

Here, the summation is over all values of $r = m-n$ for which $f_m(n) = f(m-n) = f_r(0)$ is a function of a single variable only. Using standard second order perturbation theory, with an initial state that consists of an electron of momentum $\hbar k$ and no phonons, and an intermediate state that consists of an electron with momentum $\hbar(k-q)$ and a single phonon of momentum $\hbar q$, the energy is given by

$$E = \frac{\hbar^2 k^2}{2m_0} + \sum_q \frac{\tilde{c}_q^\dagger \tilde{c}_q}{\hbar^2 (k-q)^2 = 2m_0 + \hbar \omega_q}; \quad (104)$$

where the ground state energy E_0 occurs at $k=0$ and \sum_q is a suitable Brillouin zone average.

The number of virtual phonons in the polaron cloud is defined as

$$N_{ph} = \sum_q \frac{\tilde{c}_q^\dagger \tilde{c}_q}{\hbar \omega_q}; \quad (105)$$

where $|j^0\rangle$ represents the eigenstate for the perturbed Hamiltonian. Using standard first order perturbation theory, this is given, for the case of $k=0$, by

$$N_{ph} = \sum_q \frac{\tilde{c}_q^\dagger \tilde{c}_q}{(\hbar \omega_q)^2}; \quad (106)$$

The ground state effective mass is easily found by differentiating Eq. 104 according to Eq. 95 and setting $k=0$, to give

$$\frac{m_0}{m} = 1 + 4 \sum_{q \neq 0} \frac{\tilde{c}_q^\dagger \tilde{c}_q}{(\hbar \omega_q)^3}; \quad (107)$$

Differentiating this expression according to equation (98) gives the isotope exponent on the effective mass as

$$m = 2 \frac{m}{m_0} \sum_q \left(\frac{3 \sim! j f_q j^2 \sim^2 q^2 = 2m_0}{(q^2 = 2m_0 + \sim!)^4} \frac{2 j f_q j^2 \sim^2 q^2 = 2m_0}{(\sim^2 q^2 = 2m_0 + \sim!)^3} \right) : \quad (108)$$

The above expressions for the observables may be written in the form (measuring the energy from the bottom of the free-electron band)

$$\frac{1}{t} E_0 = 2 E_0 (f; !); \quad (109)$$

$$N_{ph} = N_{ph} (f; !); \quad (110)$$

$$\frac{m_0}{m} = 1 m (f; !); \quad (111)$$

and

$$m = \frac{m_0}{m} m (f; !); \quad (112)$$

where $(f; !)$ is the coefficient of the linear term in ϵ , which may be calculated numerically. In order to do so, we make use of

$$2t - 2t \cos(ka) = \frac{\sim^2 k^2}{2m_0} + O(k^4); \quad (113)$$

which follows from Eq. 5 for small momentum. The values of $(f; !)$ for each interaction model are presented in TABLE II for $! = 1$.

Interaction Model	$f_m^2(0)$	E_0	N_{ph}	m_0/m	m
Holstein ($R_{sc} = 0$) TB	1.000	0.894	0.537	0.537	0.125
Holstein ($R_{sc} = 0$)	1.000	0.894	0.537	0.572	0.143
Screened Frohlich ($R_{sc} = 1$)	1.034	1.079	0.736	0.637	0.219
Screened Frohlich ($R_{sc} = 3$)	1.133	1.257	0.937	0.670	0.283
Non-screened Frohlich ($R_{sc} = 1$)	1.269	1.394	1.400	0.844	0.405

TABLE II: The coefficient of the linear term in ϵ in weak coupling perturbation (116{119) for the Holstein model in the one-dimensional tight-binding band, and the numerically calculated values of the coefficient of the linear term, Eqs. 109{112 in the free-electron model, for each interaction model at $! = 1$. For example, the ground state energy (109) of the Holstein polaron is given by $E_0/t = 2 \cdot 0.894$.

The coefficients can be expressed in closed form for a one-dimensional tight-binding Hamiltonian

$$H_0 = 2t \cos ka + \sim! \sum_q d_q^\dagger d_q; \quad (114)$$

with Holstein interaction. Here we find

$$E(k) = 2t \cos ka \frac{2! t}{[(! + 2 \cos ka)^2 - 4]^{1/2}} \quad (115)$$

$$E_0 (f; !) = \frac{2!}{(!^2 + 4!)^{1/2}} \quad (116)$$

$$N_{ph} (f; !) = \frac{2! (! + 2)}{(!^2 + 4!)^{3/2}} \quad (117)$$

$$m (f; !) = \frac{2! (! + 2)}{(!^2 + 4!)^{3/2}} \quad (118)$$

$$m (f; !) = \frac{!^2 (!^2 + 2! + 4)}{(!^2 + 4!)^{5/2}} \quad (119)$$

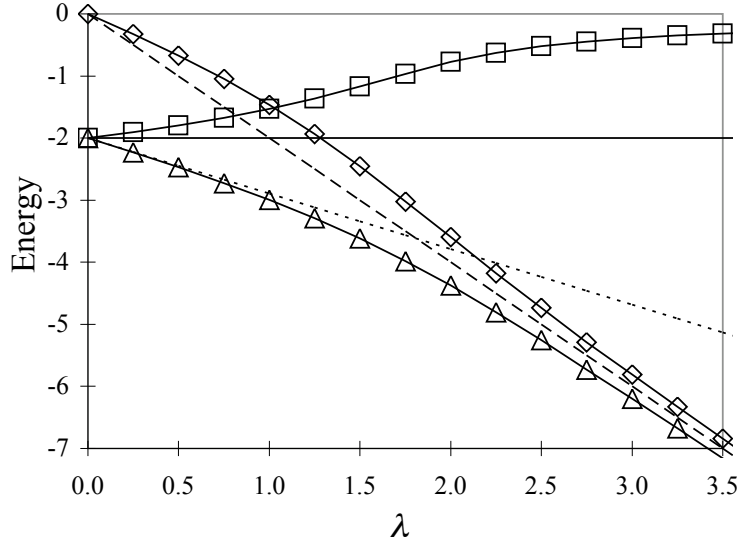


FIG. 4: The variation of ground state energy $E_0(0)$ (triangles), together with potential energy (diamonds) and kinetic energy (squares), with coupling λ for the one-dimensional Holstein model with a dimensionless phonon frequency of $\omega = 1$. The dashed line is the strong coupling perturbation (SCP) result (93) and the dotted line the weak-coupling perturbation (WCP) result (109). One can clearly distinguish the large-polaron, transition and small-polaron regions.

V I. R E S U L T S

A . H o l s t e i n I n t e r a c t i o n

1. S e l f - T r a p p i n g T r a n s i t i o n

Let us consider first the QMC results for the simplest case of the one-dimensional Holstein model. The variation of the ground state energy $E_0(0)$ with the coupling constant λ is shown in FIG. 4 for a fixed phonon frequency of $\omega = 1$. These QMC results are in excellent agreement with those obtained by independent methods (such as exact diagonalization and variational calculations), showing that the present QMC scheme is free from systematic errors. The $E_0(0)$ curve tends to the weak-coupling perturbation (WCP) result from below as $\lambda \rightarrow 0$, and to the strong-coupling perturbation (SCP) result as $\lambda \rightarrow 1$. Here we have also plotted the first and second terms of equation (83), which provide an indication of the potential energy (PE) and the kinetic energy (KE) of the system, respectively. Three separate regions can be clearly distinguished from FIG. 4:

1. The large-polaron region at weak-coupling ($\lambda = 0$ to $\lambda = 1$ in this case) is defined as the range of λ for which $E_0(0)$ is accurately described by WCP theory (section V). At $\lambda = 0$ the energy is entirely kinetic and represents the bottom of the bare-electron band (with $E_0(0) = -zt$). As λ increases within this region, KE increases but remains large compared with PE (non-localised band-electron like states).
2. The small-polaron region at strong-coupling (in this case $\lambda = 2.5$ to $\lambda = 1$) has $E_0(0)$ accurately predicted by SCP theory (section V). The PE is much greater than the KE (self-trapped states).
3. The smooth transition region at intermediate coupling ($\lambda = 1$ to $\lambda = 2.5$ in this case) between the two regions above. As λ increases in this region, a decrease in the PE and an increase in KE indicates the localization of the polaron.

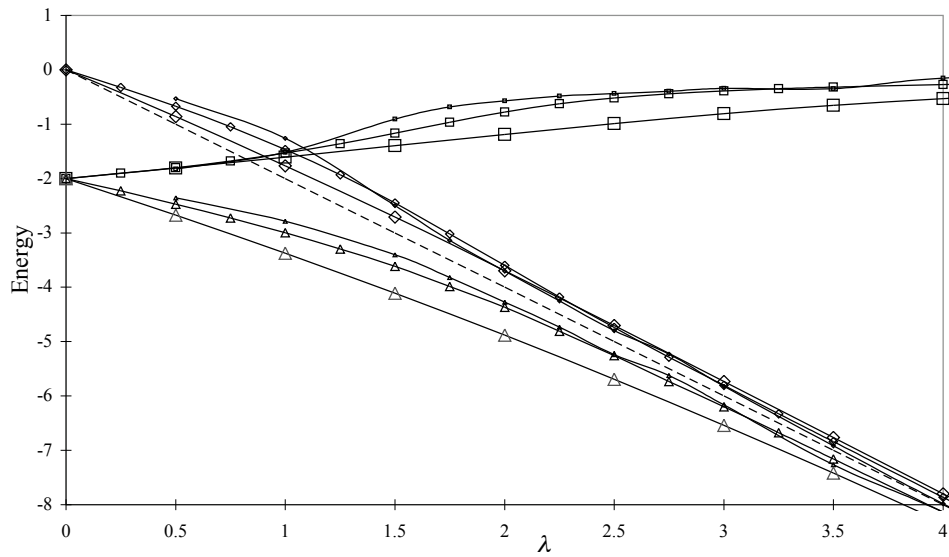


FIG . 5: The variation of ground state energy $E_0(0)$ (triangles), together with potential energy (diamonds) and kinetic energy (squares), with coupling λ , for the one-dimensional Holstein model with a phonon frequency of $\omega = 0.5$ (small symbols), 1.0 (medium-size symbols) and 3.0 (large symbols). As λ increases, the transition region shifts to higher λ and becomes broader.

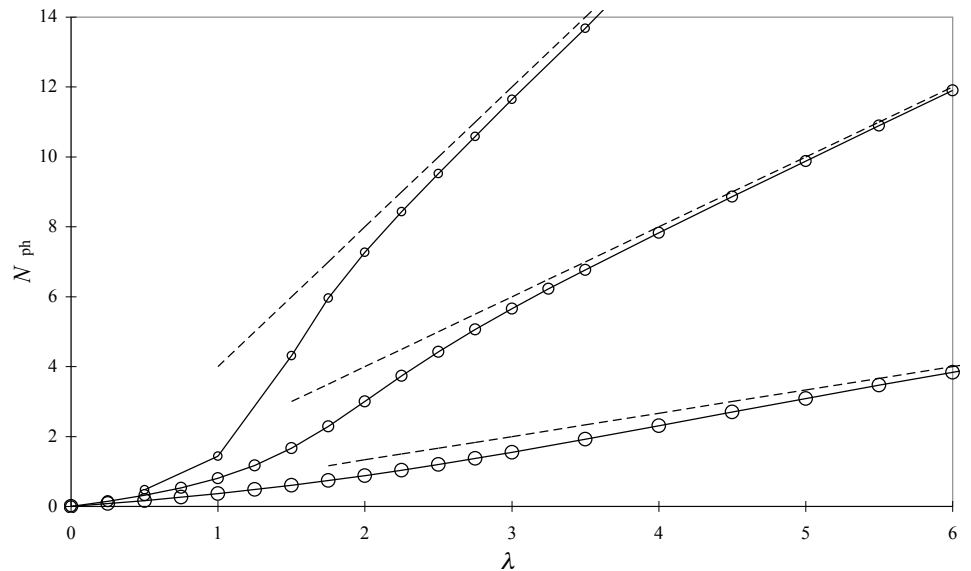


FIG . 6: The number of phonons for the Holstein model at $\omega = 0.5; 1.0; 3.0$ (small, medium-size, and large circles respectively). The dashed line shows the SCP result (93). The transition region boundaries are the same as those in FIG . 5.

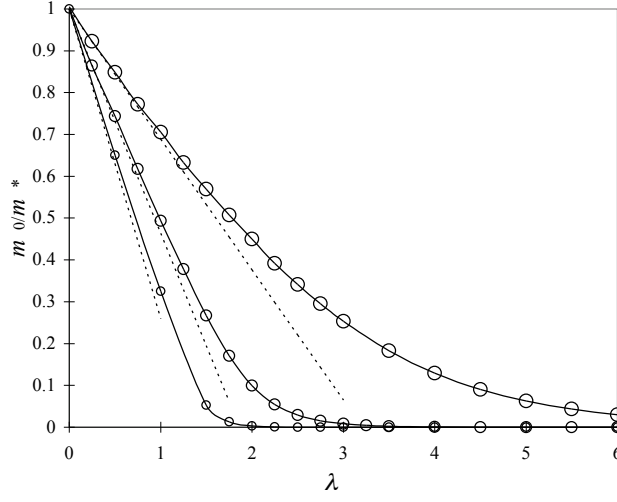


FIG . 7: The inverse effective mass m_0/m_* (where $m_0 = \hbar^2/2ta^2$ is the bare-electron mass) for the Holstein model at $\omega = 0.5; 1.0; 3.0$ (small, medium-size, and large circles respectively). The dotted line shows the WCP result (118) for the tight-binding Hamiltonian.

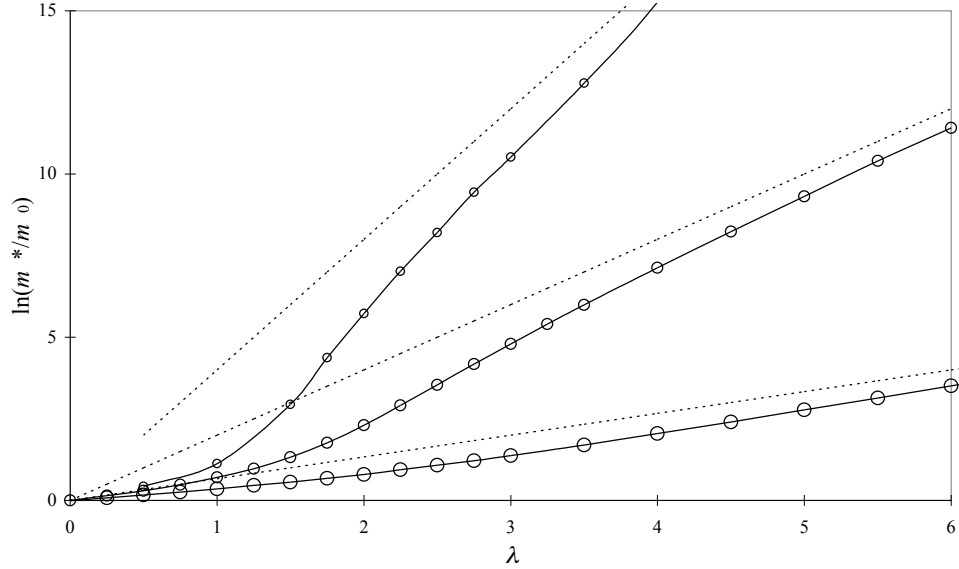


FIG . 8: The logarithm of the effective mass for the Holstein model at $\omega = 0.5; 1.0$ and 3.0 (small, medium-size, and large circles respectively). The dashed line shows the SCP result $\ln(m_*/m_0) = 2\omega$.

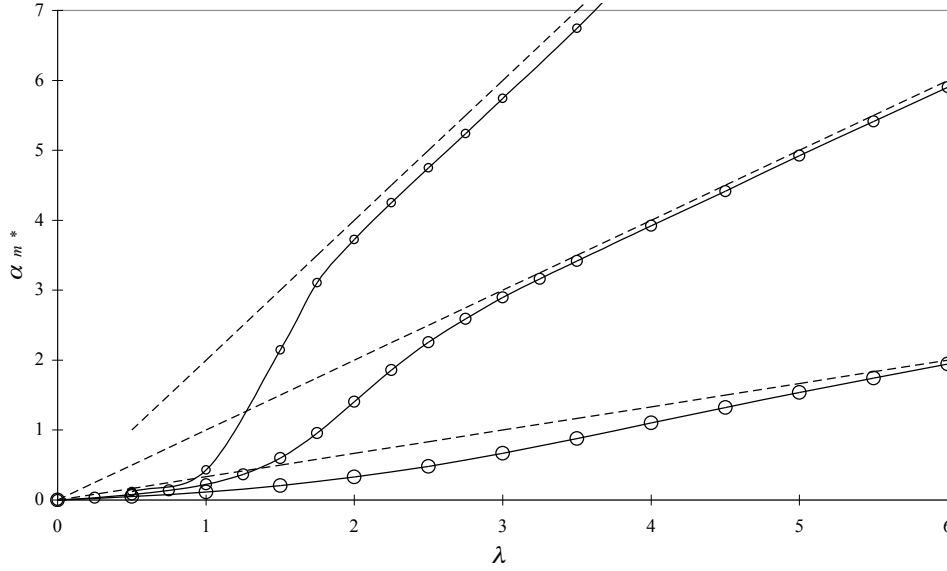


FIG . 9: The isotope exponent for the Holstein model at $\lambda = 0.5; 1.0; 3.0$ (small, medium-size, and large circles respectively). The dotted line shows the SCP result.

2. Variation with Phonon Frequency

Now let us consider the way in which the properties of the Holstein polaron are affected by altering the value of the dimensionless phonon frequency λ , as defined by Eq. 9. This quantity (also known as the adiabatic ratio) is often used as a parameter in analytical approaches to the polaron problem: the adiabatic regime is defined as the case when $\lambda < 1$, and the anti-adiabatic regime as $\lambda > 1$. With this in mind, we present below the properties of the one-dimensional Holstein polaron for $\lambda = 0.5$, $\lambda = 1$, and $\lambda = 3$.

The ground state energies for all three values of λ are presented together in FIG . 5 against β . The PE tends to the same (λ -independent) SCP result of $E_0(0) = 2$ as $\beta \rightarrow 1$. Notice that the KE for intermediate and large values of β (mainly due to that of the lattice vibrations) decreases as λ increases. This affects the position of the start and end of the transition region. More precisely, as λ increases:

1. The start of the smooth transition region moves to higher β .
2. The transition region becomes broader (the start of the small-polaron region is also shifted to larger β).

The values of β that mark the estimated start and end of the transition region are shown in TABLE III. The definition of β , in Eq. 10, is independent of λ , and so naturally characterizes the three regions defined above.

The variation of N_{ph} with β is presented in FIG . 6 for each value of λ . Over all couplings, N_{ph} decreases as the value of λ increases. Loosely speaking, it is simply "harder" to create phonons of higher frequency. The smooth transition from large to small polaron is again visible in the results for N_{ph} , with the edges of the transition region occurring at the same β as in the above results for $E_0(0)$.

The QMC results for the inverse effective mass $m_0^{-1} = m^*$, and the isotope exponent on the effective mass m_m , are presented against β in FIGS. 7{9, for each value of λ . We see from FIG . 7 that increasing λ reduces the effective mass over the entire range of β . Both $m_0^{-1} = m^*$ and m_m tend to the WCP solution as β becomes small, and to the SCP result as β becomes large. However, the results for $\ln(m_m = m_0)$ tend to the SCP solution at a slower rate than for the other observables.

From all the results for the Holstein model above, we observe that as the value of λ increases, the curve for each observable (PE, N_{ph} , m^* , and m_m) against β moves closer to the line representing the SCP result over the entire range of β . In other words, the SCP prediction becomes more applicable as λ increases.

ω	(end of large-polaron region)	(start of small-polaron region)
0.5	(1.1 0.1)	(2.0 0.2)
1	(1.3 0.1)	(2.7 0.3)
3	(2.1 0.1)	(5.5 0.6)

TABLE III: The boundaries of the transition region for the one-dimensional Holstein model at different values of the (dimensionless) phonon frequency ω . The estimates are based on the QMC results for the energies and N_{ph} (observing the changing "trend" in plots of the deviation from the corresponding SCP and WCP result).

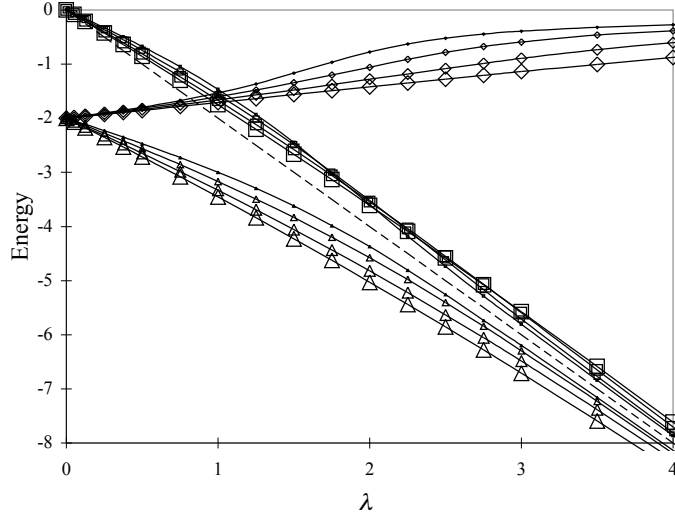


FIG. 10: The ground state energy $E_0(0)$ (triangles), potential energy (squares), and kinetic energy (diamonds) of the one-dimensional screened Frohlich model at $\omega = 1$, versus λ , for screening lengths $R_{\text{sc}} = 0; 1; 3; 1$ (increasing size of symbols). The curves for $E_0(0)$ (and PE) tends to the same strong coupling perturbation (SCP) result of $E_0 = -2$ (dashed line) as $\lambda \rightarrow \infty$. Note the crossing of the potential energy curves near $\lambda = 2$.

B. Screened Frohlich Interaction

Here we consider the case of the one-dimensional screened Frohlich model, Eq. 16, at a fixed dimensionless phonon frequency of $\omega = 1$. We investigate the way the polaron properties depend on the range of the electron-phonon interaction by comparing the QMC results at four different values of the screening length (shown in FIG. 2): $R_{\text{sc}} = 0$ (the short-range Holstein interaction), $R_{\text{sc}} = 1$, $R_{\text{sc}} = 3$, and $R_{\text{sc}} = 1$ (the non-screened Frohlich interaction).

The QMC results for the energy ($E_0(0)$, PE, and KE) and the number of phonons in the polaron cloud N_{ph} are presented against λ in FIGS. 10 and 11 respectively. They are in excellent agreement with the WCP results at small λ (not shown), and tend to the same (that is, λ -independent) SCP result as $\lambda \rightarrow \infty$. One can see that, as the value of R_{sc} increases, the KE increases less rapidly with λ , and so:

1. The start of the transition region shifts to higher λ .
2. The transition region becomes broader (in λ).

This behavior is similar to that found for the Holstein model with increasing ω . In the present case, with the phonon frequency ω fixed, the above effect is due only to changing the shape of the electron-phonon interaction force $f_m(n)$. TABLE IV shows the values of λ that mark the estimated start and end of the transition region for each value of R_{sc} . From the N_{ph} results in FIG. 11, we notice that increasing the value of R_{sc} has the effect of increasing N_{ph} at small

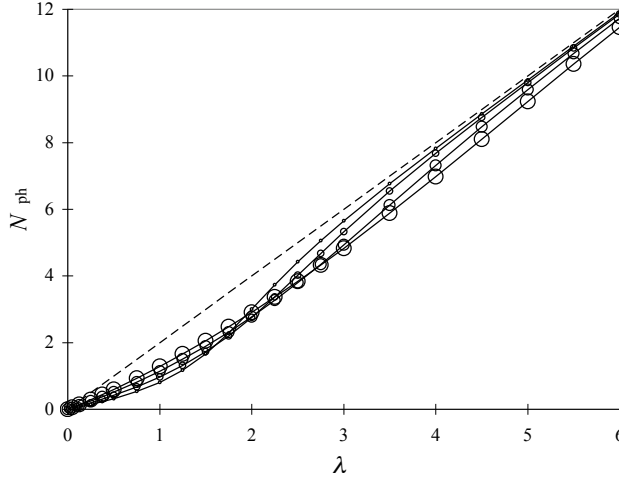


FIG . 11: The number of phonons in the polaron cloud N_{ph} versus λ for screening lengths $R_{sc} = 0;1;3;1$ (increasing size of circles) at $\beta = 1$. The curves tend to the same SCP result of $N_{ph} = z = \lambda$ (dashed line) as $\beta \rightarrow 1$.

Interaction Model	(start of transition)	(end of transition)
Holstein ($R_{sc} = 0$)	(1.1 0.1)	(2.0 0.2)
Screened Frohlich ($R_{sc} = 1$)	(1.7 0.1)	(3.8 0.4)
Screened Frohlich ($R_{sc} = 3$)	(2.2 0.1)	(4.7 0.4)
Non-screened Frohlich ($R_{sc} = 1$)	(2.9 0.2)	(6.3 0.5)

TABLE IV : The boundaries of the transition region for the one-dimensional screened Frohlich interaction, at various screening lengths R_{sc} (measured in units of the lattice constant). The estimates are based on the QMC results for the energy and N_{ph} .

, and the opposite effect of decreasing N_{ph} at large λ . That is, the order that N_{ph} appears (with increasing R_{sc}) in the large polaron region is the reverse of the order in the small polaron region.

The results for the effective mass are presented in FIGS. 12 and 13, and the isotope exponent results in FIG. 14, against λ for the same four values of R_{sc} . We can see that for each value of R_{sc} the QMC results tend to the "model dependent" SCP result (of $\ln(m^*m_0) = 2 = \lambda$ and $m^* = \lambda$), where the value of the mass enhancement factor is given in TABLE I for each R_{sc}). This model-dependency is in contrast to the above results for $E_0(0)$ and N_{ph} , which are β -independent in the limit $\beta \rightarrow 1$.

An important observation is evident from the plot of $\ln(m^*m_0)$ against λ shown in FIG. 13. At intermediate and large couplings (that is, in the transition and small polaron regions), altering the value of R_{sc} has a dramatic effect on the effective mass. For example, the non-screened Frohlich polaron is over 10^3 times "lighter" than the Holstein polaron at $\lambda = 4$, and over 10^4 times lighter at $\lambda = 5$.

The isotope exponent m^* in FIG. 14 shows a strong dependence on the range of the electron-phonon interaction (as well as on β and λ) in the (physically most realistic) intermediate values of coupling. This is encouraging, as experimental measurement (by Zhao et al.) of the exponent of the isotope exponent on the effective supercarrier mass along the CuO_2 planes, m_{ab}^* , in the material $\text{La}_{2-x}\text{Sr}_x\text{CuO}_4$ shows a large value of $m^* = 1.9(2)$ in the deeply underdoped regime ($x = 0.06$), and much smaller value of $m^* = 0.46(5)$ for optimal doping ($x = 0.15$)^{10,64}.

Now let us consider the large-polaron region. The QMC results for m^* and m^* tend to the WCP results for all R_{sc} (not shown) as $\beta \rightarrow 0$. As was the case for N_{ph} , we see from FIGS. (12 and 14) that the order that m^* and m^* appear in the large polaron region (with increasing R_{sc}) is the opposite to that in the small polaron region. As can be seen in from FIG. 12, the decrease of $m_0 = m$ with λ is approximately linear for the Holstein model, and approximately exponential for the other screening lengths. In fact, the effective mass of the Frohlich large-polaron is larger (up to

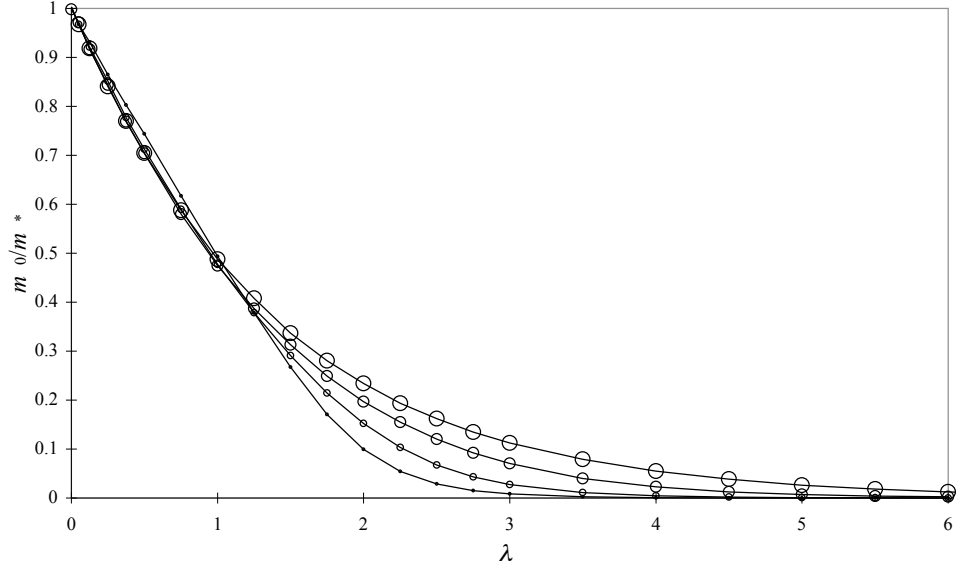


FIG .12: The inverse effective mass m_0^*/m for screening lengths $R_{sc} = 0;1;3;1$ (increasing size of circles) versus λ at fixed $\beta = 1$. For weak coupling ($\lambda < 1$) the Holstein large-polaron has a slightly smaller m_0^* than the long-range interactions.

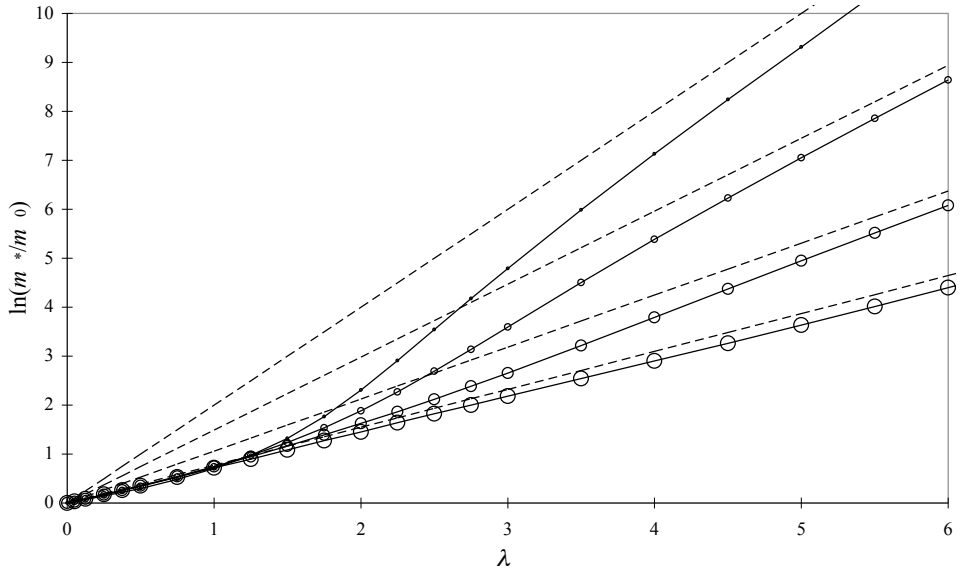


FIG .13: The logarithm of the effective mass for screening lengths $R_{sc} = 0;1;3;1$ (increasing size of circles) versus λ at $\beta = 1$. At intermediate and strong coupling, decreasing the value of R_{sc} dramatically increases the effective mass. The curves tend to the SCP result (dashed lines) at a slower rate than $E_0(0)$ and N_{ph} .

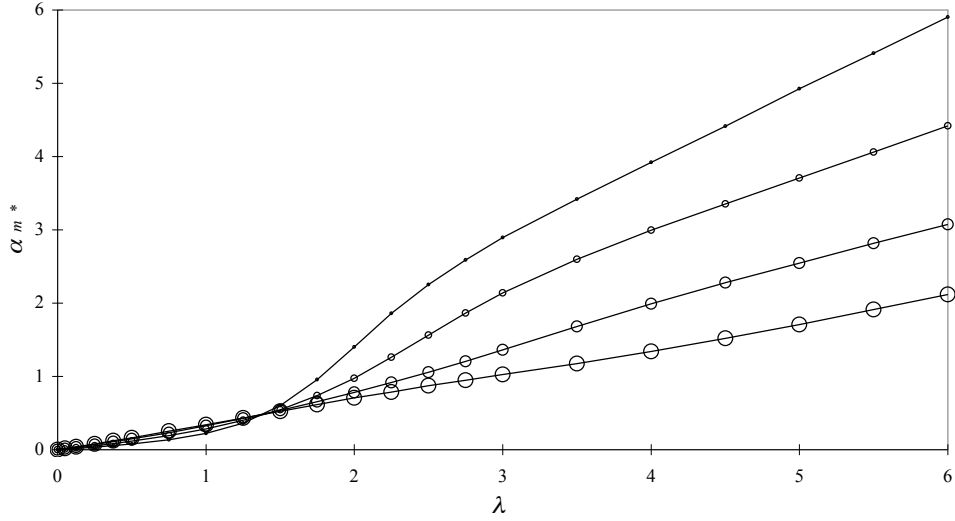


FIG. 14: The isotope exponent on the effective mass α_m^* for screening lengths $R_{sc} = 0; 1; 3; \infty$ (increasing size of circles) versus $\lambda = 1$.

approximately 10%) than the effective mass of the (short-range) Holstein large-polaron.

It is apparent from the above results for the screened Frohlich model that as R_{sc} increases (from Holstein to Frohlich), the QMC results move, in general, closer to the SCP prediction over the entire range of λ . That is, the SCP prediction becomes generally more applicable as the range of interaction increases (as well as with increasing λ). This fact allows us to define the intermediate region of the coupling strength and of the adiabatic ratio as a "small polaron" regime for any realistic-range e-ph interaction, that is the regime which is well described by the small polaron theory based on the Lang-Firsov transformed Hamiltonian averaged over phonons.

VII. CONCLUSIONS

The general aim of this work was to investigate the way in which the range of electron-phonon interaction governs the physical properties of the (single) lattice polaron. The understanding of this is of considerable current interest because of the increasing amount of experimental evidence suggesting that polarons are present in high-temperature superconducting and colossal magnetoresistance materials.

Perturbation approaches are used in the limits of strong and weak electron-phonon coupling strength λ . However, in general these do not provide an acceptable description in the (physically most realistic) intermediate coupling range.

1. We have performed an extensive Monte Carlo study of the ground state properties for the screened Frohlich polaron, equation (16), in one dimension, over a wide range of coupling.

We used path-integral quantum Monte Carlo, in which the phonon degrees of freedom are analytically integrated out, leaving only the electron coordinates to be simulated. The use of a path integral with twisted boundary conditions allowed us to extract dynamic properties directly from the simulations. There were no (systematic) errors due to finite size or finite time-step.

The properties measured were the ground state energy $E_0(0)$, the number of phonons in the polaron cloud N_{ph} , the effective mass m^* , and the isotope exponent on the effective mass α_m^* . The QMC results were always found to tend to the weak-coupling perturbation (WCP) predictions for $\lambda \rightarrow 0$, and to the strong-coupling perturbation (SCP) predictions for $\lambda \rightarrow \infty$.

The screened Frohlich polaron was studied for various values of the screening length R_{sc} (which essentially controls the range of the electron-phonon interaction): $R_{sc} \rightarrow \infty$ (on-site, Holstein interaction), $R_{sc} = 1$, $R_{sc} = 3$, and

$R_{sc} \neq 1$ (long-range, non-screened Frohlich interaction). For each value of R_{sc} , we determined the variation of the above observables with ω , at a fixed phonon frequency of $\omega = 1$. The main findings are summarized below:

1. We observed the presence of a self-trapping transition for all values of R_{sc} . In each case, the following three regions were identified:
 - (a) The large-polaron region at weak coupling, in which the behavior of the system is accurately described by WCP theory. This region is characterized by delocalized, band-electron-like states.
 - (b) The small-polaron region at strong coupling, in which the behavior is accurately described by SCP theory. This region is characterized by localized ("self-trapped") polaronic states.
 - (c) The transition region between the two, at intermediate coupling. We observed a smooth cross-over from large to small polaron in all the observables measured.
2. The transition region boundaries depend on the range of interaction. As the value of R_{sc} increased:
 - (a) The start of the transition region (the point at which it becomes energetically favorable for localized states to exist) shifts to higher ω .
 - (b) The transition region becomes broader (the start of the small polaron region also shifts to higher ω). The small-polaron region starts when the kinetic energy is much smaller than the potential energy.
 - (c) The value of the observables (PE , N_{ph} , m^* , and m) generally move closer to the corresponding SCP result over the entire range of ω .
3. In the large polaron region, the effective mass for long-range electron-phonon interaction ($R_{sc} > 1$) was found to be up to approximately 10% larger than that for the Holstein interaction ($R_{sc} \neq 0$).
4. We observed large variations in the isotope exponent on the effective mass m^* in the (physically most realistic) intermediate coupling regime (with changing R_{sc} and ω , as well as ω). This is encouraging, as experimental observation shows large variations in the isotope exponent with the level of doping in high- T_c materials.
5. Reducing the range of electron-phonon interaction dramatically increases the effective mass for intermediate and large values of coupling (that is, in the transition and small-polaron regions). In comparison, $E_0(0)$ and N_{ph} are only slightly affected by altering R_{sc} .
6. We also studied the way in which the phonon frequency ω affected the properties for the Holstein polaron ($R_{sc} \neq 0$). As ω increased:
 - (a) The transition region shifted to higher ω .
 - (b) The transition region became broader.
 - (c) The observables (PE , N_{ph} , m^* , and m) moved towards the corresponding SCP result over the entire range of ω .
7. Increasing interaction range has a qualitatively similar effect to increasing phonon frequency; compare for example FIGS. 8 and 13 or FIGS. 9 and 14.

We can also calculate the isotope effect on the whole polaron band dispersion applying the continuous-time quantum Monte-Carlo algorithm⁶⁵. To deal with the electron spectral function and high-energy excitations, involving phonon shake-off, measured in ARPES^{37,38,39}, the QMC algorithm has to include the off-diagonal paths, which remains a challenging problem.

Acknowledgments

PES acknowledges support from an EPSRC studentship, and ASA acknowledges support of the Leverhulme Trust (London).

- Electronic address: jh.samson@lboro.ac.uk
- ¹ Electronic address: pavel.komilovich@hp.com
- ² Electronic address: a.s.alexandrov@lboro.ac.uk
- ¹ H. Bottger and V.V. Bryksin, *Hopping Conduction in Solids*, Akademie-Verlag Berlin (1985).
- ² G.D. Mahan, *Many Particle Physics*, Plenum Press, (1990).
- ³ A.S.A. Alexandrov and N.F. Mott, *Rep. Prog. Phys.* 57, 1197 (1994); *Polarons and Bipolarons* (World Scientific, Singapore, 1995).
- ⁴ J.T. Devreese, in *Encyclopedia of Applied Physics*, vol. 14, p. 383, VCH Publishers (1996).
- ⁵ in *Anharmonic Properties of High-T_c Cuprates*, eds. D.M. Mihailovic et al, (World Scientific, Singapore, 1995).
- ⁶ in *Polarons and Bipolarons in High-T_c Superconductors and Related Materials*, eds E.K.H. Salje, A.S.A. Alexandrov and W.Y. Liang, Cambridge University Press, Cambridge, 353 (1995).
- ⁷ A.S.A. Alexandrov and V.V. Kabanov, *Phys. Rev. B* 54, 3655 (1996).
- ⁸ A.J.M. Illis, P.B. Littlewood, and B.I. Shraiman, *Phys. Rev. Lett.* 74, 5144 (1995).
- ⁹ A.S.A. Alexandrov and A.M. Bratkovsky, *Phys. Rev. Lett.* 82, 141 (1999).
- ¹⁰ G. Zhao, M.B. Hunt, H. Keller, and K.A. Müller, *Nature* 385, 236 (1997).
- ¹¹ A.B. Migdal, *Zh. Eksp. Teor. Fiz.* 34, 1438 (1958) (*Sov. Phys. JETP* 7, 996 (1958)).
- ¹² G.M. Eliashberg, *Zh. Eksp. Teor. Fiz.* 38, 966 (1960); *ibid* 39, 1437 (1960) (*Sov. Phys. JETP* 11, 696 (1960); 12, 1000 (1960)).
- ¹³ D.J. Scalapino, in *Superconductivity*, ed. R.D. Parks, Marcel Dekker, p. 449 (1969).
- ¹⁴ I.G. Lang and Yu.A. Firsov, *Zh. Eksp. Teor. Fiz.* 43, 1843 (1962) (*Sov. Phys. JETP* 16, 1301 (1963)).
- ¹⁵ A.S.A. Alexandrov, *Zh. Fiz. Khim.* 57, 273 (1983) (*Russ. J. Phys. Chem.* 57, 167 (1983)).
- ¹⁶ A.S.A. Alexandrov and E.A. Mazur, *Zh. Eksp. Teor. Fiz.* 96, 1773 (1989).
- ¹⁷ A.S.A. Alexandrov, *Phys. Rev. B* 46, 2838 (1992).
- ¹⁸ L.D. Landau, *J. Phys. (USSR)* 3, 664 (1933).
- ¹⁹ V.V. Kabanov and O.Yu. Mashtakov, *Phys. Rev. B* 47, 6060 (1993).
- ²⁰ A.S.A. Alexandrov, V.V. Kabanov, and D.K. Ray, *Phys. Rev. B* 49, 9915 (1994).
- ²¹ A.R. Bishop and M. Salkola, in *Polarons and Bipolarons in High-T_c Superconductors and Related Materials*, eds E.K.H. Salje, A.S.A. Alexandrov and W.Y. Liang, Cambridge University Press, Cambridge, 353 (1995).
- ²² H. Fehske, H. Roder, G.W. Ellein, and A.M. Ištarić, *Phys. Rev. B* 51, 16582 (1995).
- ²³ F. Marsiglio, *Physica C* 244, 21 (1995).
- ²⁴ Y. Takada and T. Higuchi, *Phys. Rev. B* 52, 12720 (1995).
- ²⁵ H. Fehske, J. Loos, and G.W. Ellein, *Z. Phys. B* 104, 619 (1997).
- ²⁶ T. Hotta and Y. Takada, *Phys. Rev. B* 56, 13 916 (1997).
- ²⁷ A.H. Romero, D.W. Brown and K. Lindenberg, *J. Chem. Phys.* 109, 6504 (1998).
- ²⁸ A. Lamaña and R. Pucci, *Phys. Rev. B* 53, 8449 (1996).
- ²⁹ P. Benedetti and R. Zeyher, *Phys. Rev. B* 58, 14320 (1998).
- ³⁰ T. Frank and M. Wagner, *Phys. Rev. B* 60, 3252 (1999).
- ³¹ L. Provile and S. Aubry, *S. Eur. Phys. J. B* 11, 41 (1999).
- ³² J. Bonca, S.A. Trugman, and I. Batistic, *Phys. Rev. B* 60, 1633 (1999).
- ³³ A.S.A. Alexandrov and P.E. Komilovitch, *Phys. Rev. Lett.* 82, 807 (1999).
- ³⁴ A.S.A. Alexandrov, *Phys. Rev. B* 61, 12315 (2000).
- ³⁵ A.S.A. Alexandrov, *Phys. Rev. B* 46, 14932 (1992).
- ³⁶ A.S.A. Alexandrov, Guo-meng Zhao, H. Keller, B. Lorenz, Y.S. Wang, and C.W. Chu, *Phys. Rev. B* 64, 140404 (2001).
- ³⁷ A. Lanzara, P.V. Bogdanov, X.J. Zhou, S.A. Kellar, D.L. Feng, E.D. Lu, T. Yoshida, H. Eisaki, A. Fujimori, K. Kishio, J.I. Shimoyana, T. Noda, S. Uchida, Z. Hussain, and Z.X. Shen, *Nature* 412, 510 (2001).
- ³⁸ X.J. Zhou, J. Shi, T. Yoshida, T. Cuk, W.L. Yang, V. Brout, J. Nakamura, N. Manjiva, S. Komiyama, Y. Ando, F. Zhou, W.X. Ti, J.W. Xiong, Z.X. Zhao, T. Sasagawa, T. Kakeshita, H. Eisaki, S. Uchida, A. Fujimori, Zhenyu Zhang, E.W. Plummer, R.B. Laughlin, Z. Hussain, and Z.-X. Shen, cond-mat/0405130.
- ³⁹ G.H. Gweon, T. Sasagawa, S.Y. Zhou, J. Craf, H. Takagi, D.-H. Lee, and A. Lanzara, *APS Bulletin (March Meeting 2004)*, 158; to appear in *Nature*.
- ⁴⁰ T. Gerisch, R. Munzner, and A. Reickers, *J. Statistical Phys.* 93, 1021 (1998).
- ⁴¹ P.E. Komilovitch, *Phys. Rev. Lett.* 81, 5382 (1998).
- ⁴² N.V. Prokofev and B.V. Svistunov, *Phys. Rev. Lett.* 81, 2514 (1998).
- ⁴³ H. Fehske, J. Loos, and G.W. Ellein, *Phys. Rev. B* 61, 8016 (2000).
- ⁴⁴ A.S.A. Alexandrov and C. Srichewin, *EuroPhys. Lett.* 51, 188 (2000).
- ⁴⁵ J. Bonca and S.A. Trugman, *Phys. Rev. B* 64, 094507 (2001); A.S.A. Alexandrov and P.E. Komilovitch, *J. Phys.: Condens. Matter* 14, 5337 (2002).
- ⁴⁶ D.M. Eagles, *Phys. Rev.* 130, 1381 (1963).
- ⁴⁷ T. Holstein, *Ann. Phys.* 8, 325 (1959); *Ann. Phys.* 8, 343 (1959).
- ⁴⁸ H. Fröhlich, *Adv. Phys.* 3, 325 (1954).
- ⁴⁹ H. de Raedt and A. Lagendijk, *Phys. Rev. B* 27, 6097 (1983).

- ⁵⁰ J. E. Hirsch, R. L. Sugar, D. J. Scalapino and R. Blankenbecler, *Phys. Rev. B* 26, 5033 (1982).
- ⁵¹ N. V. Prokofev, B. V. Svistunov and I. S. Tupitsyn *JETP Lett.* 64, 911 (1996).
- ⁵² N. V. Prokofev, B. V. Svistunov and I. S. Tupitsyn *J. Exp. Theor. Phys.* 87 310 (1998).
- ⁵³ B. B. Beard and U. J. Wiese *Phys. Rev. Lett.* 77 5130 (1996).
- ⁵⁴ R. P. Feynman *Statistical Mechanics* (Benjamin, Reading MA, 1972).
- ⁵⁵ J. Matthews and R. L. Walker *Mathematical Methods of Physics* (Benjamin, California, 1973)
- ⁵⁶ P. E. Komilovitch, *Phys. Rev. B* 60, 3237 (1999).
- ⁵⁷ K. Binder and D. W. Heermann 1988 *Monte Carlo Simulation in Statistical Physics: An Introduction* (Berlin:Springer).
- ⁵⁸ N. Metropolis, A. N. Rosenbluth, M. N. Rosenbluth, A. H. Teller and E. Teller, *J. Chem. Phys.* 21 1087 (1953).
- ⁵⁹ E. Maxwell, *Phys. Rev.* 78 477 (1950).
- ⁶⁰ C. A. Reynolds, B. Serin, W. H. Wright and N. Nesbitt, *Phys. Rev.* 78 487 (1950).
- ⁶¹ A. S. Alexandrov, in *Theory of Superconductivity: from weak to strong coupling*, IoP Publishing, Bristol-Philadelphia, pp. 95-158 (2003).
- ⁶² H. Fröhlich, H. Pelzer and S. Zienau, *Phil. Mag.* 41 221 (1950).
- ⁶³ S. I. Pekar, *Sov. Phys. JETP* 19 796 (1949).
- ⁶⁴ G. M. Zhao, K. Conder, H. Keller and K. A. Müller, *J. Phys. Condens. Matter* 10 40 (1999).
- ⁶⁵ P. E. Komilovitch and A. S. Alexandrov, to be published.